SeaWiFS Postlaunch Technical Report Series

Stanford B. Hooker, Editor
NASA Goddard Space Flight Center
Greenbelt, Maryland

Elaine R. Firestone, Senior Technical Editor
SAIC General Sciences Corporation
Beltsville, Maryland

Volume 13, The SeaWiFS Photometer Revision for Incident Surface Measurement (SeaPRISM) Field Commissioning

Stanford B. Hooker
NASA Goddard Space Flight Center
Greenbelt, Maryland

Giuseppe Zibordi
Jean-François Berthon
JRC Marine Environment Unit
Ispra, Italy

Sean W. Bailey
Futuretech Corporation
Greenbelt, Maryland

Christophe M. Pietras
SAIC General Sciences Corporation
Beltsville, Maryland

S.B. Hooker, G. Zibordi, J-F. Berthon, S.W. Bailey, and C.M. Pietras

ABSTRACT

This report documents the scientific activities that took place at the *Acqua Alta* Oceanographic Tower (AAOT) in the northern Adriatic Sea off the coast of Italy from 2–6 August 1999. The ultimate objective of the field campaign was to evaluate the capabilities of a new instrument called the SeaWiFS Photometer Revision for Incident Surface Measurements (SeaPRISM). SeaPRISM is based on a CE-318 sun photometer made by CIMEL Electronique (Paris, France). The CE-318 is an automated, robotic system which measures the direct sun irradiance plus the sky radiance in the sun plane and in the almucantar plane. The data are transmitted over a satellite link, and this remote operation capability has made the device very useful for atmospheric measurements. The revision to the CE-318 that makes the instrument potentially useful for SeaWiFS calibration and validation activities is to include a capability for measuring the radiance leaving the sea surface in wavelengths suitable for the determination of chlorophyll *a* concentration. The initial evaluation of this new capability involved above- and in-water measurement protocols. An intercomparison of the water-leaving radiances derived from SeaPRISM and an in-water system showed the overall spectral agreement was approximately 8.6%, but the blue-green channels intercompared at the 5% level. A blue-green band ratio comparison was at the 4% level.

1. INTRODUCTION

The SeaWiFS Project has emphasized in-water calibration and validation exercises (Hooker and McClain 2000) and demonstrated a total uncertainty in the measurement of in-water apparent optical properties (AOPs) at approximately the 3% level (Hooker and Maritorena 2000). The majority of the measurements have been made in Case-1 waters during oceanographic cruises as part of the Atlantic Meridional Transect (AMT) Program (Aiken et al. 2000). AMT cruises occur twice a year on board the Royal Research Ship (RRS) *James Clark Ross* (JCR) as it transits between the United Kingdom and the Falkland Islands (approximately 100° of latitude and 75° of longitude). The cruise tracks cross a wide range of ecosystems and biophysical regimes, within which conditions vary from subpolar to tropical, and from eutrophic shelf seas and upwelling systems to oligotrophic mid-ocean gyres. Although the large diversity in oceanic regimes represents a significant sampling advantage for calibration and validation activities, the amount of time available for station work is limited (which is frequently the case for long cruises, because a large amount of time must be allocated for transiting).

The SeaWiFS Project also relies on the Marine Optical Buoy (MOBY) for calibration and validation data. Buoys are excellent platforms for the production of long time series and complement the space series provided by oceanographic cruises (like the AMT Program). MOBY is sited off the Hawaiian island of Lanai and uses multiple in-water sensors to provide spectral estimates of water-leaving radiance, $L_W(\lambda)$. Although bio-fouling is always a problem for autonomous in-water systems, MOBY is situated in very clear (Case-1) water and is visited regularly, so the submerged sensors can be cleaned. The big advantage of the MOBY system is it delivers data autonomously in between the servicing visits.

The Project receives time series data from a collaboration with the Joint Research Centre (JRC) which has been making monthly visits of approximately 5-days duration to the *Acqua Alta* Oceanographic Tower (AAOT) to collect atmospheric plus marine optical and biogeochemical measurements (Zibordi et al. 2000). Traditionally, water-leaving radiances at the site were derived from in-water measurements. More recently, above-water measurements of the sea surface were added to determine whether or not a continuously operating above-water system could be implemented at the AAOT. If this proves feasible, the autonomous measurement strengths of a buoy system could be duplicated without the problems associated with biofouling.

There are disadvantages with in-water techniques which are not present in above-water methods, e.g., the self shading of the instrument itself (Gordon and Ding 1992). Not surprisingly, the latter presents new problems that are not present in the former, so there is a danger of simply swapping one set of challenging problems for another. The possibility of taking data while underway, sampling in a shorter amount of time, or autonomously monitoring a location in between site visits, however, makes the above-water instruments too useful to be ignored. For coastal sites, like the AAOT, there is another possible advantage associated with above-water measurements. In these waters, particularly those dominated by sediment loading, there is a need for measurements of water-leaving radiance in the red part of the spectrum. The large attenuation of light in the near-infrared poses significant challenges for in-water measurements, whereas the above-water methods are not so disadvantaged.

The SeaWiFS Field Team has been incrementally engaging in above-water measurements with the objective of extracting the largest amount of validation data from both measurement types. The deployments involved were

1

called SeaWiFS Bio-Optical Algorithm Round-Robin (Sea-BOARR) experiments, because the long-term objective is to evaluate the effects of the different measurement protocols on bio-optical algorithms. The SeaBOARR field campaigns have been concerned with collecting simultaneous above- and in-water radiometric measurements. The intercomparison goals for these deployments were to: a) use multiple surface glint correction methods to compute $L_W(\lambda)$ from above-water data; b) use different in-water profiling systems and analysis methods to compute $L_W(\lambda)$ (one making measurements at a fixed distance from the tower, 7.5 m, and the other at variable distances up to 29 m away); and c) compare the $L_W(\lambda)$ values estimated from the above- and in-water measurements.

SeaBOARR-98 took place on the AAOT (Hooker et al. 1999) and SeaBOARR-99 took place on the JCR during the AMT-8 cruise (Hooker and Lazin 2000). The primary reasons for selecting the AAOT for SeaBOARR-98 were the ongoing use of the tower by a group of optical oceanographers (JRC) and it can accommodate the simultaneous deployment of a large number of instruments. The other reasons were: a) its stability (towers do not pitch and roll like ships); b) the perturbative effects of the tower on the in-water light field were being studied and modeled, so a correction scheme for the in-water measurements was possible (Zibordi et al. 1999); and c) its proximity to a strong coastal front, so the water around the tower can be Case-1 or Case-2. The opportunity for sampling different water types within one field campaign was very appealing.

The experience acquired during the SeaBOARR campaigns reaffirmed the need for a low-cost, autonomous system for making above-water radiance measurements. A review of possible design concepts by the SeaWiFS Field Team resulted in the idea that a low-risk approach would be to adapt an existing automated sun photometer system to the problem. The SeaWiFS Photometer Revision for Incident Surface Measurements (SeaPRISM) is based on a CE-318 sun photometer, which is an automatic system that measures the direct sun irradiance plus the sky radiance in the sun and almucantar planes. The JRC worked with the manufacturer, CIMEL Electronique (Paris, France), to develop a capability for measuring the radiance leaving the sea surface after the sun and sky measurement sequences.

A prototype SeaPRISM was delivered in the summer of 1999; a team of scientists (Appendix A) was deployed to the AAOT shortly thereafter from 2–6 August 1999. The purpose of the campaign was to make above- and in-water radiometric measurements in support of two activities:

a) Continue an ongoing time series of bio-optical measurements that are used by the Coastal Atmosphere and Sea Time Series (CoASTS) and the SeaWiFS Projects for algorithm validation and bio-optical research; and

b) Collect a high quality data set of simultaneous above- and in-water radiometric measurements, along with a suite of bio-optical parameters for evaluating the capabilities of the SeaPRISM instrument.

2. INSTRUMENTATION

The AAOT is located in the northern Adriatic Sea (12.51°E,45.31°N) approximately 15 km east of the city of Venice (Italy). The tower was built in 1970 and is operated by an institute of the *Consiglio Nazionale delle Ricerche*† (CNR) in Venice. The water depth immediately below the tower is about 17 m and the composition of the nearby sea floor is primarily sand and silt. The tower is composed of four levels supported by four large pillars. Each level is approximately 7.2 m×5.2 m in size with the exception of the lowest level which is 5.2 m×5.2 m.

The first (lowest) tower level, about 4.5 m above the water, has an open grid deck and no facilities. The second level is approximately 7 m above the water and contains a portable scientific laboratory. At this level, a special open grid platform, 3.5 m wide, extends 6.5 m over the sea towards the southeast; the Wire-Stabilized Profiling Environmental Radiometer (WiSPER) package is deployed from this platform. Also located on this level is the water filtering and hydrography laboratory. The third deck contains the main laboratory, which is also the primary accomodations and work space. The fourth (uppermost) deck, about 13 m above the water, contains a wide variety of meteorological instruments and support facilities. A complete description of the AAOT is available in Hooker et al. (1999).

For the SeaPRISM field commissioning, WiSPER and four different radiometric systems were deployed on the AAOT:

a) The JRC miniature NASA Environmental Sampling System (miniNESS),

b) The SeaWiFS Underway Surface Acquisition System (SUnSAS),

c) The new SeaPRISM instrument, and

d) The Satellite Validation for Marine Biology and Aerosol Determination (SIMBAD) handheld radiometer.

Detailed descriptions of each of the sampling systems are given in Sects. 2.1–2.6, respectively, so only brief introductions are given here. The two in-water profilers were mini-NESS and WiSPER; SUnSAS, SeaPRISM, and SIMBAD made above-water measurements.

The SUnSAS, WiSPER, and miniNESS instruments all use 7-channel ocean color radiance series 200 (OCR-200) sensors, as well as 7-channel ocean color irradiance series 200 (OCI-200) sensors. Both radiometers use 16-bit analog-to-digital (A/D) converters and are capable of detecting light over a four-decade range. A benefit of assembling (nearly) identical equipment from the participating investigators was the wavelengths and (10 nm) bandwidths for the different instruments were very similar. A summary

---

† National Research Council.

S.B. Hooker, G. Zibordi, J-F. Berthon, S.W. Bailey, and C.M. Pietras

Table 1. Channel numbers (λ_i) and center wavelengths (in nanometers) for the radiometers used with the radiometric sampling systems. The Satlantic sensors are given with their individual sensor codes, which are formed from a one-letter designator for the type of sensor, plus a three-digit serial number (S/N). The M099 WiSPER reference was used with miniNESS, SUnSAS, and WiSPER. All of the WiSPER, miniNESS, and SUnSAS sensors have 10 nm bandwidths. The SeaPRISM and SIMBAD bandwidths are given in parentheses (the former are nominal values and did not have filters installed for channels 6 and 7).

λ_i	WiSPER				miniNESS			SUnSAS		Sun Photometers	
	R046	I071	I109	M099	R067	I097	I098	T028	T068	SeaPRISM	SIMBAD
1	412.3	412.4	412.5	411.5	412.5	412.3	412.4	412.7	412.3	1018 (10)	442.7 (11.3)
2	442.8	443.5	442.2	442.8	442.2	442.1	443.5	443.1	442.8	870 (10)	492.1 (10.5)
3	490.5	490.6	490.7	489.9	490.0	490.5	490.8	489.5	490.1	668 (10)	562.3 (8.5)
4	510.8	509.1	509.8	510.3	510.3	510.3	509.9	510.1	510.3	440 (10)	672.1 (9.7)
5	554.9	555.9	554.7	554.5	554.5	554.5	554.7	554.8	555.7	501 (10)	872.3 (12.8)
6	665.8	665.4	664.8	664.8	665.4	665.7	664.9	780.6	780.1		
7	683.9	682.1	683.2	683.2	684.0	683.8	683.2	865.4	864.3		
8										936 (10)	

of the radiometer wavelengths and their sensor codes is given in Table 1.

The WiSPER system measured upwelled irradiance and radiance plus downward irradiance as a function of depth, $E_u(z,\lambda)$, $L_u(z,\lambda)$, and $E_d(z,\lambda)$, respectively. A separate sensor measured the total solar irradiance (the direct plus the indirect or diffuse components) just above the sea surface, $E_d(0^+,\lambda)$. An occulter or *lollipop* was periodically used at the conclusion of some casts to block the direct solar irradiance, so the indirect (or diffuse) component, $E_i(0^+,\lambda)$, could be measured. WiSPER was slowly winched up and down the water column between two taught wires, so it had no need for tilt sensors.

The miniNESS profiler makes the same measurements as WiSPER, $E_u(z)$, $L_u(z)$, and $E_d(z)$, except it is deployed as a tethered, free-fall package. Internal tilt sensors quantify the vertical orientation (φ) of the profiler as it falls through the water. It is a variant of the Low-Cost NASA Environmental Sampling System (LoCNESS) and is built from the same modular components as WiSPER: a DATA-100 (with 16-bit A/D converters) for power and telemetry, and 7-channel OCR-200 and OCI-200 sensors. The main difference between LoCNESS and miniNESS is the former has the light sensors mounted at the ends of the profiler close to the centerline of the rocket-shaped body, whereas the latter has the E_d and L_u sensors mounted on the fins and the E_u sensor is mounted at the end of an extension bracket on the nose.

The SUnSAS instruments measured the sky (or indirect) radiance reaching the sea surface, $L_i(0^+)$, and the (total) radiance right above the sea surface, $L_T(0^+)$. The latter is composed of three terms: the radiance leaving the sea surface from below (the so-called water-leaving radiance), the direct sunlight reflecting off the surface (the so-called sun glint), and the skylight reflecting off the surface (the so-called sky glint). A separate sensor measured

$E_d(0^+)$ which, in this case, was the same sensor used with miniNESS (the output of the irradiance sensor was sent to both data acquisition systems).

SeaPRISM is an eight-channel radiometric system made by CIMEL Electronique (Paris, France). The CE-318 is an automated, robotic system that measures the direct sun irradiance plus the sky radiance in the sun and almucantar planes. The data are transmitted over a satellite link, and this remote operation capability has made the device very useful for atmospheric measurements. The revision to the CE-318 that makes the instrument potentially useful for SeaWiFS calibration and validation activities is to include a capability for measuring the radiance leaving the sea surface in wavelengths suitable for the determination of chlorophyll *a* concentration (C_a). Depending on the level of success achieved with the field commissioning, the current prototype will be validated in an extended (one year) deployment to determine the longer term capabilities of the instrument.

SIMBAD is a five-channel, handheld radiometer designed and manufactured by the *Laboratoire d'Optique Atmosphérique* (Lille, France). It is both an above-water radiometer and a sun photometer. It can measure water-leaving radiance in the sea-viewing mode and aerosol optical thickness in the sun-viewing mode. The same optics—filters, detectors, and 3° full-angle field of view (FOV)—are used in both measurement modes with each mode having a separate electronic gain. A vertical polarizer is used to reduce the reflected skylight and glint from the sea surface reflectance measurements. The polarizer remains in place during the sun measurements, but because the direct radiation is not polarized, the sun measurements are still accurate.

A summary of each sensor system, including their sensor types, primary physical measurements, and sensor codes, is given in Table 2. SeaPRISM and SIMBAD were

the only integrated (all-in-one) systems using the same optics for each type of measurement—the other systems were built up from modular components involving multiple sensor types.

Table 2. A summary of the radiometers used during the SeaPRISM field test along with their primary physical measurement (in terms of their vertical sampling), their spectral resolution (λ_5 means 5 channels, λ_6 means 6 channels, and λ_7 means 7 channels), and their sensor codes. The M099 sensor was periodically occulted to measure $E_i(0^+, \lambda_7)$. The ϕ coordinate is the solar azimuth angle and ϑ is the radiometer pointing angle with respect to the vertical axis, z.

System	Sensor	Measurement	Code
WiSPER	OCR-200	$L_u(z, \lambda_7)$	R046
	OCI-200	$E_d(z, \lambda_7)$	I071
	OCI-200	$E_u(z, \lambda_7)$	I109
	OCI-200	$E_d(0^+, \lambda_7)$	M099
miniNESS	OCR-200	$L_u(z, \lambda_7)$	R067
	OCI-200	$E_d(z, \lambda_7)$	I097
	OCI-200	$E_u(z, \lambda_7)$	I098
	OCI-200	$E_d(0^+, \lambda_7)$	M099
SUnSAS	OCR-200	$L_i(0^+, \lambda_7)$	T068
	OCR-200	$L_T(0^+, \lambda_7)$	T028
	OCI-200	$E_d(0^+, \lambda_7)$	M099
	DIR-10	ϑ, ϕ	D002
SeaPRISM	CE-318	$E(0^+, \lambda_6)\dagger$	
	CE-318	$L_i(0^+, \lambda_6)\dagger$	
	CE-318	$L_T(0^+, \lambda_6)\dagger$	
SIMBAD	SIMBAD	$E(0^+, \lambda_5)$	
	SIMBAD	$L_T(0^+, \lambda_5)$	

† The operational unit will have 8 wavelengths (λ_8).

The basic data sampling activity involved collecting data from the above- and in-water instruments as simultaneously as possible, so handheld radios were used to coordinate the beginning and ending of sampling intervals. The main synchronization of the sampling was between the above-water instruments, because these systems were sufficiently similar or flexible to make this possible. The in-water systems were simply used as rapidly as possible to ensure good overlap with the above-water data. The basic data collection differences between the various sampling systems were the time required to complete a cast and the sampling rate.

Although it would have been preferable to have all of the instruments sample the smallest patch of water possible, space limitations on the tower did not permit this. The SUnSAS and SeaPRISM instruments had to be mounted on the topmost deck, which had a number of superstructure obstacles (wind generator, antenna masts, etc.), so the southwest side was selected to minimize any negative effects on the light measurements. The SIMBAD instrument

was used in close proximity to SUnSAS and SeaPRISM to ensure the three above-water systems were sampling approximately the same water.

In addition to paying close attention to the optimal viewing capabilities of each instrument system, some instruments were equipped with sensors that measured their pointing angles. SUnSAS, for example, had an external module that measured the vertical (two-axis) tilts and horizontal (compass) pointing of the radiometers (the so-called DIR-10 unit); miniNESS had internal sensors that measured the vertical (two-axis) tilts of the radiometers, and SIMBAD had a combination light and sensor system to visually indicate when the radiometer was correctly pointed (at 45° with respect to nadir). A generalized coordinate system for these pointing systems is given in Fig. 1.
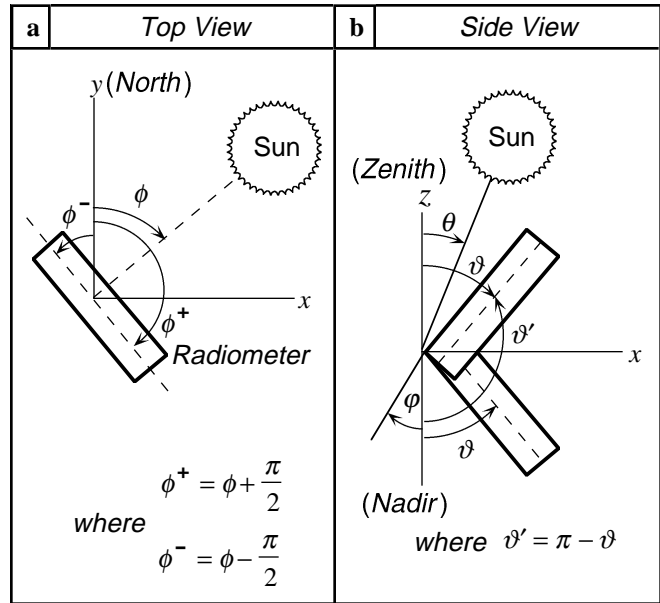
Fig. 1. The coordinate systems used for instrument pointing: **a)** looking down from above (the z-axis is out of the page), and **b)** looking from the side (the y-axis is out of the page). The ϕ coordinate is the solar azimuth angle, θ is the solar zenith angle, and ϑ is the radiometer pointing angle with respect to the vertical axis, z. The perturbation (or tilt) in vertical alignment, which can change the pointing angles, is given by φ.

Note that ϕ is measured with respect to an arbitrary reference, in this case due north, and ϑ is measured with respect to nadir (the direction pointing straight down to the sea surface). The angle ϑ' corresponds to the angle ϑ measured with respect to the zenith (the direction pointing straight up from the sea surface). To keep the pointing nomenclature compact, the angle the radiometer is pointed with respect to the sun is considered to be ϕ', and in most cases, this was perpendicular to the sun plane: $\phi' = \phi \pm 90°$ (i.e., ϕ' was usually set to ϕ^+ or ϕ^-)

In addition to the above- and in-water optical measurements, a variety of other data were collected to help

characterize the optical properties of the site during the field campaign:

1. Seawater temperature and salinity with a conductivity, temperature, and depth (CTD) sensor, plus tide level;

2. Seawater attenuation and absorption profiles at nine wavelengths by AC-9 measurements;

3. Pigment analyses using the high performance liquid chromatography (HPLC) technique;

4. Direct sun irradiance and sky radiance measurements by CE-318 measurements;

5. *In vivo* spectral absorption of particulate matter (PM) and colored dissolved organic matter (CDOM) through spectrophotometric techniques;

6. Atmospheric pressure, humidity, and temperature, plus wind speed and direction; and

7. Total suspended matter (TSM) through gravimetric filter analysis.

The relative deployment locations of the various optical systems on the AAOT are shown in Fig. 2.
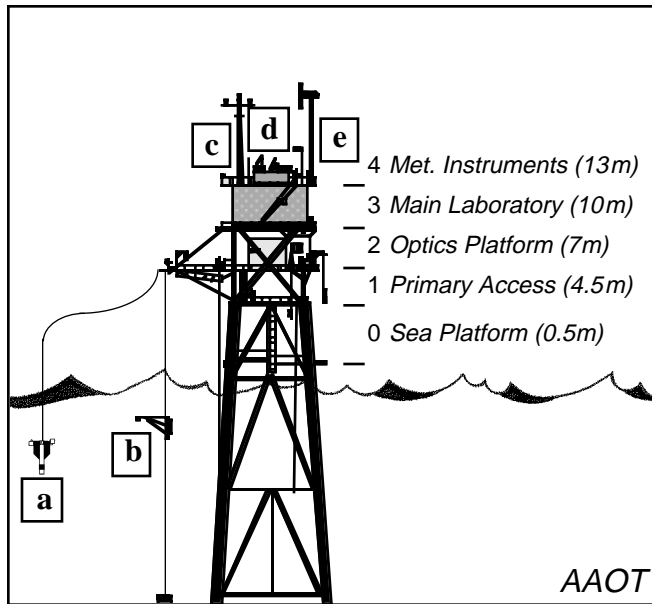
Fig. 2. The AAOT showing the mounting locations of the radiometric instruments: a) miniNESS (the irradiance reference sensor for miniNESS and SeaSAS was deployed on a mast located on the fourth deck), a) miniNESS, b) WiSPER, c) SIM-BAD, d) SUnSAS, and e) SeaPRISM. The different levels are shown on the right with their heights above the water.

2.1 miniNESS

The miniNESS profiler is a tethered free-falling instrument. It is a variant of the LoCNESS profiler first used on AMT cruises (Robins et al. 1996). An in-air irradiance sensor (M099) measured the incident solar irradiance just above the sea surface, $E_d(0^+, \lambda)$ which was periodically occulted to provide $E_i(0^+, \lambda)$ data. The irradiance sensor was packaged with a DATA-100 module that converted the analog output of the OCI-200 radiometer to RS-485 serial communications. The sensor package was mounted on a mast on the topmost tower deck (eastern corner). The height and location of the mast ensured none of the tower's superstructure shadowed the sensor under almost all illumination conditions. A schematic of the instruments used with the miniNESS profiler is given in Fig. 3.
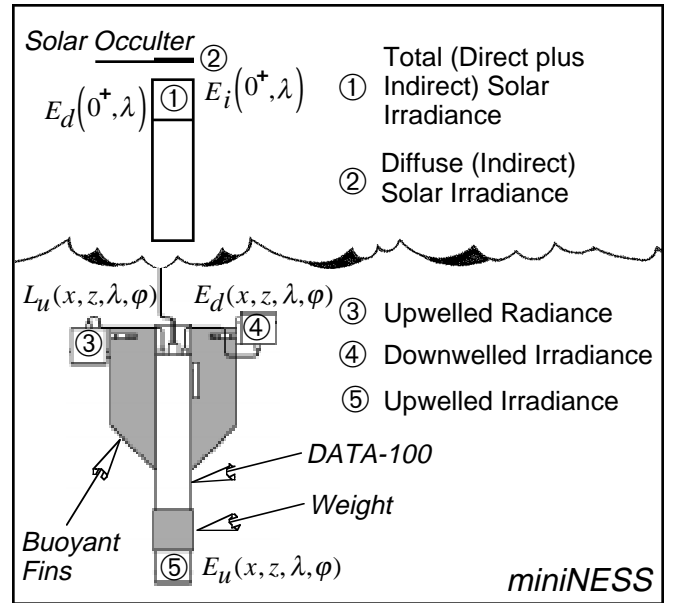
Fig. 3. A schematic of the miniNESS profiler. The solar irradiance data were provided by the WiSPER reference.

The free-fall aspects of the miniNESS design are derived from the LoCNESS profiler which was built out of modular, low-cost components: a DATA-100 (with 16-bit A/D converters) for power and telemetry, and 7-channel OCR-200 and OCI-200 sensors. In the LoCNESS configuration, the DATA-100 and the two light sensors are connected in line using extension brackets, with the OCR-200 at the nose, and the OCI-200 at the tail. The addition of weight to the nose and buoyant (foam) fins to a tail bracket produces a rocket-shaped package that falls through the water with minimum tilts (less than $2°$). The power and telemetry cable extends through the FOV of the irradiance sensor, but the small diameter of the cable (7 mm) minimizes any negative effects on the measured light field.

The LoCNESS profiler can also be built with the Three-Headed Optical Recorder (THOR) option, in which case an adapter plate is used on the nose to permit the mounting of two sensors rather than one: the usual $L_u(z, \lambda)$ sensor plus an additional $E_u(z, \lambda)$ sensor. The LoCNESS profiler is 1.78 m long with the light sensors separated by the DATA-100 and the extension brackets. This is not an optimal configuration for the shallow, Case-2 water frequently

encountered at the AAOT site, so a more compact (0.73 m long) profiler was produced by dispensing with the extension brackets, mounting a radiance sensor (R067) on one fin, and an irradiance sensor (I097) on the fin opposite the radiance sensor. As with LoCNESS, the light sensors send their analog signals to a DATA-100 (S/N 8), which digitizes them (16 bits) and converts the counts to RS-485 serial communications.

Mounting light sensors on the fins destabilizes the profiler (although, tilts less than 2° were regularly achieved on AMT cruises by carefully trimming the profiler with lead weight), and it makes the L_u sensor more susceptible to shading. This problem was minimized by choosing where the mechanical termination was with respect to the sensors and the sun. In general, the two sensor fins, which are 180° apart, will align perpendicular to the mechanical termination when the cable is pulled in to bring the profiler to the surface (before a profile). To minimize L_u sensor shading, all that is required is to choose which of the other two fins should be used for the mechanical termination, so the L_u sensor aligns towards the sun. A picture of miniNESS on the AAOT deployment platform is shown in Fig. 4.

Fig. 4. A picture of the miniNESS profiler on the AAOT deployment platform. Note, the platform floor is an open grid which helps reduce the shading effects of the tower, but does not eliminate it.

The experimental setup for deploying miniNESS began with siting a marker buoy approximately 90 m from the southeast tower leg, and displaced approximately 2 m to the side of the WiSPER instrument. A taught line was then attached from the uppermost deck of the tower to the buoy anchor, and a pulley was attached at the point where the line intersected the sea surface (about 30 m from the tower). Another pulley was mounted on the southeast corner of the tower near the sea surface, and a closed loop

of line with marks on it every 1 m was strung between the pulleys. The miniNESS profiler, was moved to a selected distance from the tower leg by pulling on the closed loop of line until the desired number of cable marks between the ring's position and the tower leg was achieved.

The versatility of measuring three components of the light field with the THOR configuration for LoCNESS is also possible with the JRC miniNESS, because of the addition of an E_u (I098) sensor on the nose of the profiler. The miniNESS profiler is sufficiently easy to handle that it can be deployed by one person. Under normal circumstances, the handler keeps a few coils of the power and telemetry cable in the water, so the profiler can fall freely through the water column; once the desired depth has been reached, the cast is terminated, and the profiler is pulled back to the surface. A cable block, which could not pass through the cable ring, was used to prevent the profiler from going deeper than 15 m and accidently impacting the sea floor.

The RS-485 signals from the two DATA-100 units were combined in a Satlantic deck box and converted to RS-232 communications for computer logging. The deck box also provided computer-controlled power for the sensors and was designed to avoid any damage due to improper power-up sequences over varying cable lengths or cable faults.

2.2 WiSPER

The WiSPER system is permanently installed on the AAOT and was operated from the 6.5 m platform extension on the second level. WiSPER used a custom-built profiling rig, and the positioning of the equipment on the rig ensured the radiometers did not view any part of the mechanical supports (which were all painted black). The rigidity and stability of the rig was carefully considered, so there was no need for tilt or roll sensors. WiSPER uses the same kind of optical sensors as miniNESS: one OCI-200 (I071) to measure $E_d(z, \lambda)$, one OCI-200 (I109) to measure $E_u(z, \lambda)$, and one OCR-200 (R046) to measure $L_u(z, \lambda)$. Two taut wires, anchored between the tower and a weight on the sea bottom, prevented the movement of the rig out of the vertical plane defined by the wires.

The WiSPER optical sensors were mounted on a retractable boom, which put them approximately 1 m away from the main part of the frame and the ancillary instruments (the AC-9, DATA-100, etc.). Once deployed, the boom placed the light sensors about 7.5 m from the nearest tower leg (the boom, as well as the entire deployment frame, could be raised to permit easy access to all of the sensors and ancillary equipment). The narrow geometry of the rig was designed to provide a minimal optical cross section. The FOV of the irradiance sensor was obstructed by the power and telemetry cable, as well as the stabilization wires, but all of these had very small cross sections and the cables were more than 1 m away from the sensors, so any negative effects were minimized.

A DATA-100 (S/N 5) provided the A/D and telemetry capability for the WiSPER light sensors. The equipment

was powered directly from 12 V lead-acid batteries which are stored and kept charged on the tower. WiSPER was raised and lowered from the southeastern side of the tower by an electrical winch, although, the power and telemetry cables were spooled out and taken in by hand (an easy exercise because of the shallow water depth). The typical speed of the winch was approximately $0.1\,\mathrm{m\,s^{-1}}$, so the vertical sampling resolution of the system was very good. A generalized schematic of what WiSPER measured is presented in Fig. 5, and a picture of the WiSPER system being deployed is shown in Fig. 6.
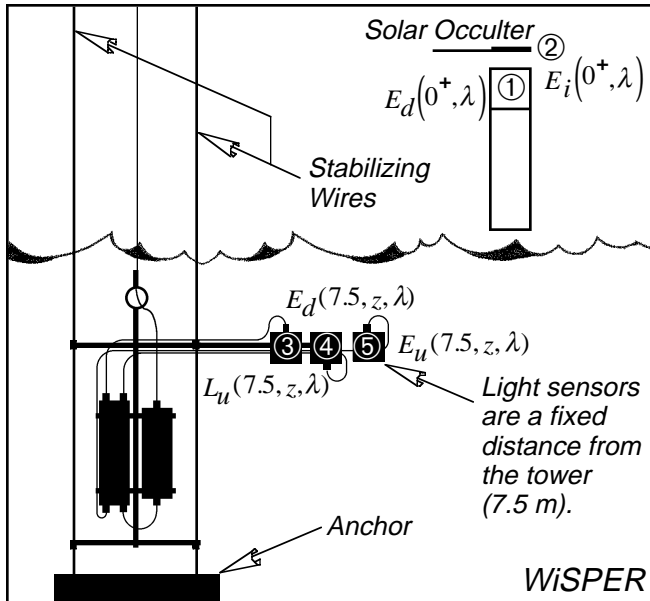
Fig. 5. A schematic of the WiSPER system. At the conclusion of the in-water sampling, the solar irradiance, $E_d(0^+, \lambda)$, sensor was occulted, so $E_i(0^+, \lambda)$ data could be collected.

Fig. 6. A picture of the WiSPER system immediately before being lowered into the sea.

During most stations on the AAOT, at least one pair of down-and-up WiSPER profiles are made each time a measurement sequence is initiated. For the SeaPRISM field commissioning, multiple optical profiles were made to ensure the maximum number of overlapping measurements with the above-water systems. The WiSPER frame also contained an AC-9, which was logged simultaneously with the light sensors on personal computers (PCs) using software supplied by the manufacturers.

The instrument self-shading correction of the in-water WiSPER data required seawater absorption, $a(\lambda)$, data and measurements of $E_i(0^+, \lambda)$ collected by periodically occulting the solar irradiance sensor. Both types of data were needed to apply the Gordon and Ding (1992) correction scheme as parameterized as a function the sun zenith angle by Zibordi and Ferrari (1995), and further parameterized by the size of the sensor by Mueller and Austin (1995).

A field campaign was performed from 3–21 July 1997, to estimate the shading effect induced on the in-water optical measurements by the AAOT (Doyle and Zibordi 1998). Sequences of downward irradiance and upwelling radiance profiles were collected at varying distances from the tower to evaluate the tower-shading effects as a function of the deployment distance. The tower-shading field data, as well as results from a Monte Carlo model, indicated the shading effect at 555 nm during clear-sky conditions was negligible for both downward irradiances and upwelling radiances at deployment distances greater than 15 m and 20 m, respectively.

At closer distances to the tower, for example at the 7.5 m deployment distance regularly used for the collection of WiSPER data, the shading effect was significant: at 555 nm during clear-sky conditions and a relatively low sun zenith angle of 22°, the shading effect was approximately 2% for downward irradiance and about 8% for upwelling radiance. These large effects indicated a correction method was needed for in-water optical data collected near the tower, if the 5% uncertainty objectives of the SeaWiFS Project were to be achieved. Consequently, a correction method based on Monte Carlo simulations was formulated (Zibordi et al. 1999).

2.3 SUnSAS

The SUnSAS data acquisition frame is a compact instrument mounting system wherein the light sensors are mounted on two plates, one large and one small, which can be tilted to the desired nadir and zenith angles. The entire platform can be rotated 360° in the azimuthal plane, and a band, marked in 2° and 5° increments, allows for a precise positioning of the frame with respect to the sun. For the SeaPRISM field commissioning, the mounting plates were mechanically secured at the desired viewing angles using aluminum wedges cut at the appropriate angles (this ensured excellent repeatability whenever the viewing angles were changed).

7

The large mounting plate was designed to accommodate the downward-viewing light sensor (T028) that measured $L_T(\lambda)$, and the small plate was designed for a solitary OCR-200 sensor (T068) that was always pointed upwards to measure $L_i(\lambda)$. Although the azimuth angle was varied to address a variety of experimental objectives, the majority of the data were collected for $\phi' = \phi \pm 90°$. The nadir and zenith viewing angles varied between $\vartheta = 30$, 40, and 45°. The SUnSAS frame included a square aperture situated within the FOV of the sea surface sensor. The aperture was designed so a plaque, usually gray, could be inserted before (or after) each surface-viewing sequence (the plaque was not used during the SeaPRISM field commissioning). The miniNESS in-air irradiance sensor was used to measure the total solar irradiance (M099). A generalized schematic of what SUnSAS measured is shown in Fig. 7.

Fig. 8. A picture of the SUnSAS frame on the topmost platform of the AAOT showing the square aperture for plaque measurements (not made during the SeaPRISM commissioning) and the two radiometers pointed towards the sea and sky. The cylinder in the background is the DIR-10.
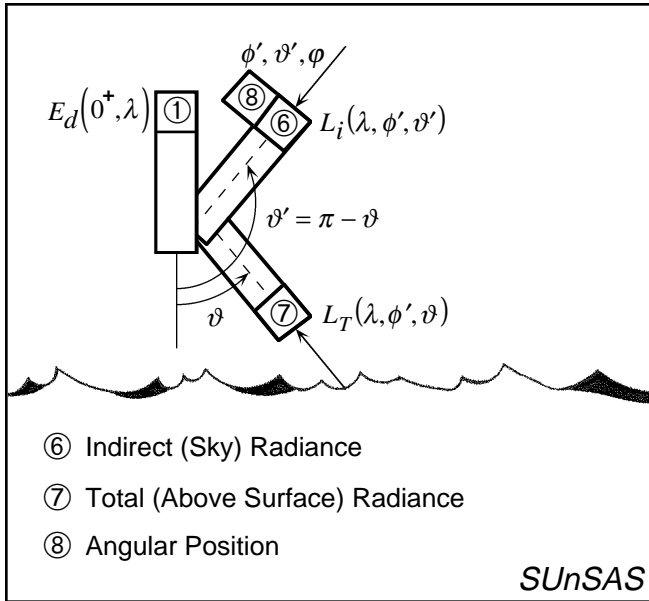
Fig. 7. A schematic of the SUnSAS instruments. The solar irradiance measurements were provided by the miniNESS reference.

The radiometers used with SUnSAS were connected in a modular fashion. The T028 sensor was integral to a DATA-100, whereas, the T068 sensor was cabled to a separate DATA-100, which was also cabled to the DIR-10. All of the sensors were powered by the same deck box, so the sensors took and reported data simultaneously (via RS-485 serial communications). As with miniNESS, the RS-485 signals from the two DATA-100 units were combined in the deck box and converted to RS-232 communications for computer logging. The RS-232 data were logged on a Macintosh PowerBook computer using software developed at the University of Miami Rosenstiel School for Marine and Atmospheric Science (RSMAS) and the SeaWiFS Project. A side view of SUnSAS deployed on the topmost platform of the AAOT is shown in Fig. 8.

The two data streams (above- and in-water measurements) were time stamped and recorded to disk simultaneously. The data were stored as American Standard Code for Information Interchange (ASCII), tab-delimited (spreadsheet) files, so they could be viewed easily. The operator controlled the logging and display of the data as a function of the acquisition activity: dark data (caps on the radiometers), sea and sky viewing, etc. The initiation of the execution mode automatically set the file name and file headers, as well as the timed termination of the data aquisition. All of the telemetry channels were displayed and visualized in real time.

2.4 SIMBAD

SIMBAD is a handheld radiometric package that is powered by an internal rechargeable battery with a 6 h lifetime†. An external global positioning system (GPS) sensor is provided and connected to the radiometer to supply location information for the collected data. Temperature and viewing angles (yaw, pitch, and roll) are also acquired during the measurement sequences from internal sensors. The yaw sensor did not work properly during the SeaPRISM commissioning, so a handheld digital compass was used to point the instrument properly with respect to the sun.

---

† A complete description of SIMBAD and its capabilities are available at `http://genius.ucsd.edu/~simbad/`.

SIMBAD makes two types of environmental measurements: during the sun-viewing mode, the direct solar irradiance, $E(\lambda, \phi, \theta)$, is measured, and during the sea-viewing mode $L_T(\lambda, \phi \pm 135°, 45°)$ is measured. The sun and sea surface data are collected and stored internally before they are downloaded in a computer communications mode. Five spectral bands centered at approximately 443, 492, 562, 672, and 872 nm are used in the two normal collection modes. A schematic of what SIMBAD measured is shown in Fig. 9.
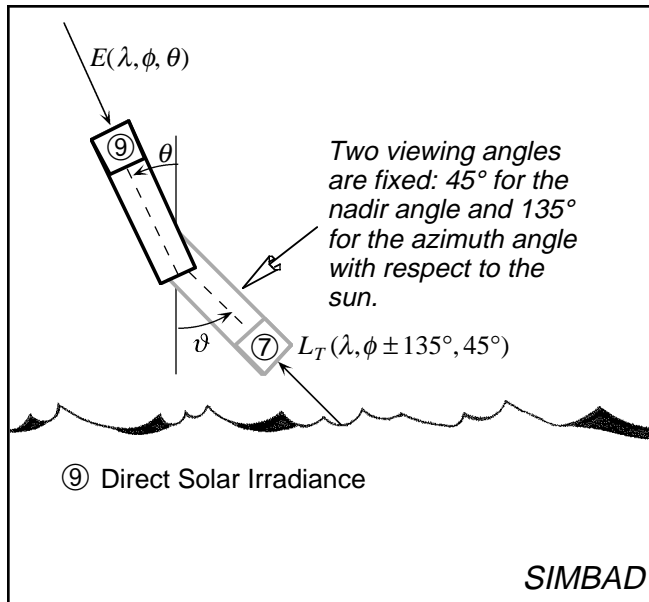
Fig. 9. A schematic of the SIMBAD system. The same instrument is used to make the $E(\lambda)$ and the $L_T(\lambda)$ measurements (so the latter is shown stippled).

A special mode of operation is designed to measure the *dark* or bias voltages at the detectors when they are not illuminated. Dark voltages need to be collected before and after each sea- and sun-viewing measurement. Additional modes exist for instrument calibration and computer downloads, and the user manually selects the desired mode. It takes 10 s to collect a measurement in the sun- and sea-viewing modes, whereas it takes 20 s in the dark and calibration modes.

SIMBAD operates at 10 Hz, and for reflectance measurements, all 100 samples during the 10 s sampling interval are recorded. To minimize sun-pointing errors on a moving platform during sun photometry measurements, only the highest radiances measured during each second of the 10 s sampling interval are recorded. During dark mode measurements, 10 records are stored for each electronic gain; each dark record is the average of the data collected during the 1 s measurement interval. A picture of SIMBAD being used on the topmost platform of the AAOT is shown in Fig. 10.

Fig. 10. A picture of the handheld SIMBAD instrument being used on the topmost platform of the AAOT (note the SUnSAS instrument in the background).

2.5 SeaPRISM

The CE-318 sun photometer is a fully autonomous system operating on batteries that are kept charged with solar panels. A large number of CE-318 sun photometers have been used successfully as part of the Aerosol Robotic Network (AERONET) with many deployed in remote (island) locations (Holben et al. 1998). In-water moored systems based on buoys, are the traditional platform for the deployment of autonomous oceanographic measurements. Offshore platforms capable of accommodating above-water instruments are ubiquitous features of the coastal environment and offer significant advantages over a buoy:

a) A reduction in the vulnerability of the sensors (the structure, and thus the entire sensor system, is not easily harmed by recreational or commercial activities);

b) A simplification in the powering of the equipment (many offshore structures have power systems already installed);

c) An increase in the pointing stability of the sensors (the sensors are not subjected to the ocean wave field);

d) An almost complete reduction in the fouling of the optical surfaces (the primary source of fouling is wind-blown particles); and

e) A simplification in maintaining and cleaning the equipment (most offshore structures provide easy access for authorized personnel).

The SeaPRISM configuration is the same as the standard instrument except an additional sea-viewing capability was added to the usual sun- and sky-viewing modes.

SeaPRISM data were collected during the three acquisition scenarios using two different collimators: sun (sun collimator), sky (sky collimator), and sea (sky collimator). During the sun-viewing mode $E(\lambda, \phi, \theta)$ was measured for the retrieval of aerosol optical thickness; during the sky-viewing mode, the sky radiance, $L_i(\lambda)$, was measured in a wide range of angles in the almucantar and sun planes for the retrieval of the aerosol scattering phase function; and during the sea-viewing mode, $L_i(\lambda, \phi', \vartheta')$ and the total radiance immediately above the sea surface, $L_T(\lambda, \phi', \vartheta)$, were measured for estimating water-leaving radiance.

The sea-viewing measurements were made at pointing angles suitable for the estimation of water-leaving radiances: $\vartheta = 30, 40,$ and $45°$; $\vartheta' = 150, 140,$ and $135°$; and $\phi' = \phi^+$ and $\phi' = \phi^-$. In the standard instrument, the measurement gains are set and defined in firmware. The same is true for the sea-viewing measurement, because the sea and sky radiances are performed using the same gains, but different gains can be used for sea and sky. During each sea-viewing sequence, three values of $L_i(\lambda)$ or $L_T(\lambda)$, depending on the pointing angle, were sequentially collected at each λ for each successive ϑ at $\phi' = \phi^+$ and then $\phi' = \phi^-$. A schematic of what SeaPRISM measured is shown in Fig. 11.
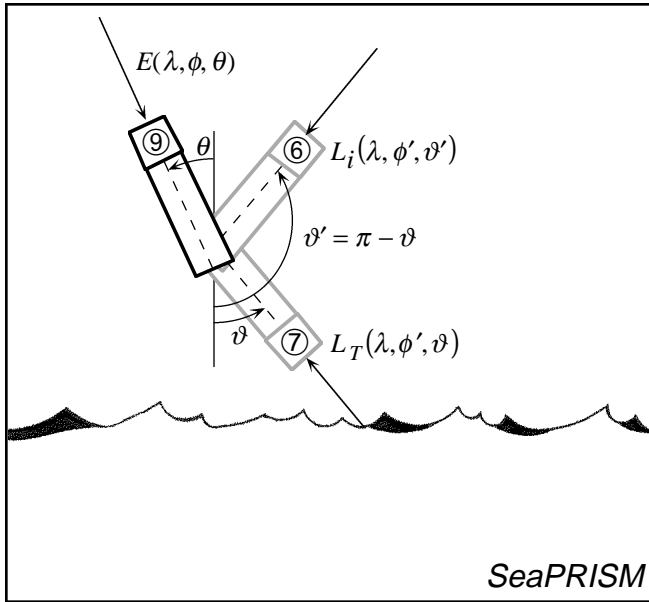
Fig. 11. A schematic of the SeaPRISM system. The same instrument is used to make the $E(\lambda)$, $L_i(\lambda)$, and $L_T(\lambda)$ measurements (the latter two are shown stipled).

To simplify the command structure for implementing the water-leaving radiance protocol in the instrument, the sea-viewing measurement began at $\vartheta = 30°$, and continued through $\vartheta = 40, 45, 135, 140, 150, 210, 220, 225, 315, 320,$ and $330°$. The first pair of three measurements give $L_T(\lambda)$ and $L_i(\lambda)$, respectively, at $\phi' = \phi^+$; and the last pair of three measurements give $L_i(\lambda)$ and $L_T(\lambda)$, respectively,

at $\phi' = \phi^-$. A sea-viewing measurement sequence lasted approximately 3 min. Dark measurements were taken by capping the entrance aperture of the radiometer (normally these data would be collected using the so-called *field stop* on the filter wheel).

Although the standard CE-318 instrument telemeters the data over a satellite link, the prototype used during the field commissioning did not have this capability—all of the data were downloaded after acquisition to a PC from the central processing unit using a serial interface. The data were subsequently processed using a processing package developed at the JRC. A picture of SeaPRISM during a sea-viewing measurement is shown in Fig. 12.

Fig. 12. The SeaPRISM instrument being used on the topmost platform of the AAOT. The collimators are the two long tubes pointed towards the sea, and the box in the foreground contains the central processing unit and rechargeable batteries.

3. IN-WATER METHODS

The sampling procedures used with the in-water systems were a direct consequence of the various acquisition sequences and measurement protocols associated with each instrument, coupled with the mixture of the investigative objectives and the analysis procedures. For the purposes of defining and then categorizing the various activities involved, a *cast* was defined as either an acquisition sequence of the sky (and sun if applicable) plus the sea surface from the above-water instruments, or a vertical profile of the water column from the in-water instruments. An *experiment* was defined as a separate series of casts collected to investigate a specific investigative objective, e.g., variable nadir or zenith viewing angle, variable azimuthal angle with respect to the sun plane, etc.

The in-water analysis techniques commonly in use are based primarily on the Smith and Baker (1984) method.

S.B. Hooker, G. Zibordi, J-F. Berthon, S.W. Bailey, and C.M. Pietras

The ultimate purpose of the in-water approach is to extrapolate the measured subsurface properties up to, and then through, the sea surface interface. Vertical sampling close to the sea surface, like that which can be achieved with the WiSPER system, ensures the needed amount of data to establish confidence in the extrapolation interval and procedure. The steps involved are as follows:

1. Compute K_u, the diffuse attenuation coefficient calculated from $L_u(z, \lambda)$ profiles, as the local slope of $\ln\left[L_u(z, \lambda)\right]$ in a depth interval of a few meters centered on depth z_0 (Smith and Baker 1984 and 1986):

$$\ln\left[L_u(z, \lambda)\right] = \ln\left[L_u(z_0, \lambda)\right] - K_u(z_0, \lambda)\delta z, \quad (1)$$

where $\delta z = z - z_0$. The unknowns, $\ln\left[L_u(z_0, \lambda)\right]$ and $K_u(z_0, \lambda)$, are determined as the intercept and slope of a least-squares linear regression to the measured $\ln\left[L_u(z, \lambda)\right]$ data within the depth interval $z_0 - \Delta z \leq z < z_0 + \Delta z$. The half interval Δz is somewhat arbitrary, although, $2\Delta z \approx 2$–5 m for WiSPER data.

2. Extrapolate $L_u(z_0, \lambda)$ up to the surface using

$$L_u(0^-, \lambda) = L_u(z_0, \lambda) \exp\left[z_0 K_u(z_0, \lambda)\right]. \quad (2)$$

3. Transmit $L_u(0^-, \lambda)$ through the sea surface according to Austin (1974) to derive the in-water $L_W(\lambda)$ value:

$$\tilde{L}_W(\lambda) = \frac{1 - \rho(\lambda, \vartheta)}{n_w^2(\lambda)} L_u(0^-, \lambda), \quad (3)$$

where $\rho(\lambda, \vartheta)$ is the Fresnel surface reflectance and $n_w(\lambda)$ is the refractive index of seawater (all the in-water instruments use nadir-viewing radiance sensors for which $\vartheta = 0°$).

Austin (1980) noted the $\left(1 - \rho(\lambda, \vartheta)\right)n_w^{-2}(\lambda)$ expression can be replaced by a constant, because the wavelength dependence of the variables is very weak. The coefficient 0.54 has been shown to be the most appropriate for transmitting the normal radiance from below to above the sea surface (Mobley 1999).

4. ABOVE-WATER METHODS

The main difficulty with above-water measurements is associated with correcting the observations for the effect of surface waves which introduce significant fluctuations into the glint and reflected skylight components of the surface radiance field. The problem is made more difficult by the presence of clouds which increase the fluctuations and associated uncertainties in the measurements. At present, there are several methods for surface glint correction which were developed for different environmental conditions, i.e., clear or cloudy sky, and Case-1 or Case-2 water. All of the

methods recognize the importance of making surface measurements free of sun glint effects, so the differences in the methods are primarily due to how sky glint contamination is removed from the surface signal.

Some above-water techniques attempt to deal with the negative effects of glint at the point of measurement, like the SIMBAD radiometer (Fougnie et al. 1999a), but most methods attempt to deal with glint explicitly by filtering it out or removing it with a correction algorithm. The Mueller and Austin (1995) SeaWiFS protocol, hereafter referred to as S95, is one of the methods to prescribe a glint filter as part of the method.

The primary difference in the above-water measurement sequences was in the pointing angles. For the SUnSAS and SeaPRISM instruments, the nadir (sea-viewing) and zenith (sky-viewing) angles were varied between 30, 40, and 45°, although 40° was the most common for the former; SIMBAD always used a fixed nadir angle of 45°. The other angle that was varied was the azimuthal angle with respect to the sun. SUnSAS used a large variety of angles between 90–135°, and SeaPRISM always collected data at $\phi\pm90°$; again, SIMBAD used a fixed angle of $\phi+135°$.

When the above-water systems were used together, they usually collected data simultaneously with the WiSPER and miniNESS instruments. During each sequence, the following parameters were recorded by the operator(s):

a) The azimuthal orientation relative to the sun plane, plus the nadir and zenith angles;

b) The sky conditions around the sun (cloud coverage and haze thickness);

c) Sea surface conditions in the region observed by the sea-viewing sensor (amount of sun glint and foam, wave height, surface roughness, etc.);

d) Sky conditions in the region of the sky observed by the sky-viewing sensor (cloud coverage and haze thickness); and

e) General environmental conditions important to the measurements and not covered above.

All of this information was incorporated (where appropriate) into the various electronic logs kept for each sampling system.

4.1 SUnSAS Protocols

The first revision of the SeaWiFS Ocean Optics Protocols incorporated new protocols in several areas, including expanded protocol descriptions for Case-2 waters and other improvements, as contributed by several members of the SeaWiFS Science Team (Mueller and Austin 1995). The version 1 revision required the following for making above-water radiometric measurements for estimating $L_W(\lambda)$:

1. The radiometer measuring water-leaving radiance should point to the sea surface with an angle of about $\vartheta = 20°$ from nadir and away from the solar azimuth angle (ϕ) by at least 90°, i.e., ϕ'.

2. Foam and floating material must be avoided during measurements, and because of temporal variability due to waves, it is important to record a number of spectra within a period of a few seconds (e.g., 30 spectra within 15 s).

3. Before calculating final mean and standard deviation spectra, outliers should be removed by computing initial estimates of these statistics and rejecting radiance spectra containing values more than 1.5 standard deviations ($1.5\,\sigma$) from the estimated mean (μ).

4. $L_T(\lambda)$ must be corrected for sky glint using measurements of sky radiance, $L_i(\lambda)$, in the direction appropriate for the specular reflection from the sea surface into the sensor. $L_i(\lambda)$ measurements can be made either by looking at a horizontal *first surface* mirror (a mirror with no layers other than the reflective surface) at the same nadir and azimuth angles used for the $L_T(\lambda)$ observations, or by pointing the radiometer into the sky at a zenith angle equal to the nadir angle of the $L_T(\lambda)$ observations (or as in Fig. 1, $\vartheta' = \pi - \vartheta$) and with the same azimuth angle. The sky glint is removed from $L_T(\lambda)$ using $\rho(\lambda, \vartheta)$ to retrieve the above-water $L_W(\lambda)$ values:

$$\hat{L}_W(\lambda) \;=\; L_T(\lambda, \phi', \vartheta) \;-\; \rho(\lambda, \vartheta) L_i(\lambda, \phi', \vartheta'). \quad (4)$$

From 11–12 December 1997, the Normalized Remote Sensing Reflectance (NRSR) Workshop was held at the Center for Coastal Physical Oceanography, Old Dominion University [see Hooker et al. (1999) for a summary of the discussions and conclusions regarding above-water measurements agreed to at this meeting]. Radiative transfer simulations of remote sensing reflectance measurements above a wave-roughened surface, which were presented by Mobley (1999), showed the increase with wind speed (and resulting surface wave slope) of sky radiance and sun glint reflectance in total radiance viewed at the sea surface, relative to radiance from beneath the surface. At wind speeds approaching $10\,\mathrm{m\,s^{-1}}$, the superior nadir (and azimuth) viewing angle was $40°$, rather than the $30°$ used by many of the participants (and the $20°$ given in the original publication of the S95 protocol). At lower wind speeds and a $40°$ viewing angle, an effective surface reflectance of $\rho' = 0.028$ was recommended.

Based on the consensus reached at the NRSR Workshop, all of the SUnSAS measurements in the SeaBOARR field campaign used a viewing angle of $40°$ with respect to the vertical except when specific experiments were executed to vary the viewing angle. Accordingly, the S95 protocol was updated as follows:

$$\hat{L}_W(\lambda) \;=\; L_T(\lambda, \phi', \vartheta) - \rho' L_i(\lambda, \phi', \vartheta'). \quad (5)$$

Every effort was made to adhere to these same sampling criteria for the SeaPRISM field commissioning, except a diversity of nadir, zenith, and azimuthal angles were purposefully incorporated into the prototype unit, so the importance of pointing angles could be assessed.

4.2 SIMBAD Protocols

The efficiency of measuring the polarized components of the marine reflectance to reduce the skylight reflection effect in above-water measurements was presented by Fougnie et al. (1999a). The SIMBAD radiometer was designed to exploit this concept, and was used for calibrating the ocean color spectral bands of the Polarization Detecting Environmental Radiometer (POLDER) satellite sensor (Fougnie et al. 1999b).

SIMBAD measurements need to be made under clear-sky conditions. Cloud coverage must be less than 2/8 and must not obscure any part of the solar disk. Measurements need to be taken at a nadir angle of $45°$ and an azimuth angle of $135°$ relative to the sun plane to avoid the glitter region. This configuration permits minimization of the reflected skylight, as well as residual ocean polarization effects.

When solar radiation enters the Earth's atmosphere, a part of the incident light is attenuated through scattering and absorption processes. The solar irradiance $E(\lambda)$ measured at an observation point (assumed here to be at sea level) can be expressed as a function of the extraterrestrial solar irradiance, $E_0(\lambda)$, as:

$$E(\lambda) \;=\; E_0(\lambda) e^{-m\tau(\lambda)}, \quad (6)$$

where τ is the total atmospheric optical thickness and m is the relative air mass computed using the Kasten and Young (1989) formulation.

In the absence of absorption by water vapor and uniformly mixed gases, τ can be decomposed into the sum of the optical thickness of each major optical component of the atmosphere (at the wavelengths of interest):

$$\tau(\lambda) \;=\; \tau_{R}(\lambda) \;+\; \tau_{O}(\lambda) \;+\; \tau_{A}(\lambda), \quad (7)$$

where the R subscript stands for the Rayleigh component (molecules of the air), O for the ozone, and A for the aerosols, respectively.

A Langley calibration was used to determine the $E_0(\lambda)$ value in digital counts at each wavelength, $D_0(\lambda)$. Intercalibrations are also performed at the Goddard Space Flight Center (GSFC) with a reference sun photometer calibrated at Mauna Loa, Hawaii. The aerosol optical thickness (AOT) values are retrieved in the 443, 490, 560, 670, and 870 nm wavelengths using the calibration data and the direct solar measurements performed during the sun-viewing mode:

$$\tau(\lambda) = \frac{\ln\big[D_0(\lambda)\big] - \ln\big[D^L(\lambda) - D_D^L(\lambda)\big] - \ln\left[\dfrac{d_0^2}{d^2}\right]}{m(\theta)}, \quad (8)$$

where d_0^2/d^2 provides the Earth–sun distance correction, and $D_D^L(\lambda)$ is the dark voltage in counts for the low-level gain.

The wavelength dependency of the AOT is commonly expressed by the Ångström law (Ångström 1929) as

$$\tau_A(\lambda) = \beta\lambda^{-\alpha}, \qquad (9)$$

where α and β are the Ångström exponent and coefficient, respectively. The downward irradiances, $E_d(0^+, \lambda)$, are estimated as follows:

$$E_d(0^+, \lambda) = E_0'(\lambda)\, t_a(\lambda)\, (1 + T_C), \qquad (10)$$

where $E_0'(\lambda)$ are the solar irradiances (given for each SIM-BAD channel in $W\, m^{-2}\, mm^{-1}$) which are corrected for the solar zenith angle (θ) and the Earth–sun distance using

$$E_0'(\lambda) = E_0(\lambda)\cos(\theta)\left[\frac{d^2}{d_0^2}\right]; \qquad (11)$$

$t_a(\lambda)$ is the atmospheric transmittance estimated by (Tanré et al. 1979 and Deschamps et al. 1983)

$$t_a(\lambda) = e^{-m[0.48\tau_R(\lambda) + 0.17\tau_A(\lambda) + \tau_O]}; \qquad (12)$$

and T_C is the cloud coverage correction factor, which is computed as

$$T_C = \frac{f_{cc}\left(1 - e^{-\tau_C/2}\right)}{2\cos(\theta)}, \qquad (13)$$

where f_{cc} is the fractional cloud coverage estimated by the user during the measurements, and τ_C is the cloud optical thickness. For cumulus (cu-type) clouds, τ_C typically has a value of 5.

The observed marine reflectance values, $\rho_0(\lambda)$, are retrieved from measurements taken during the sea-viewing mode:

$$\rho_0(\lambda) = \frac{C_F(\lambda)\left(D^H(\lambda) - D_D^H(\lambda)\right)}{\cos(\theta)}\left[\frac{d^2}{d_0^2}\right], \qquad (14)$$

where $D_D^H(\lambda)$ are the dark voltages in the high-level gain, and $C_F(\lambda)$ is the calibration factor in reflectance per numerical counts.

The observed reflectances are then corrected for the skylight reflection to determine the polarized marine reflectance, $\rho_m^{//}(\lambda)$:

$$\rho_m^{//}(\lambda) = \frac{\rho_0^{//}(\lambda) - \rho_c^{//}(\lambda)}{t_a(\lambda)}, \qquad (15)$$

where $\rho_c^{//}(\lambda)$ and $\rho_0^{//}(\lambda)$ are the parallel polarized components of the skylight reflectance and the observed reflectance, respectively.

The skylight reflection correction is improved using the 870 nm channel. The reflectance at 870 nm should be zero. The measurement is rejected if the reflectance at 870 nm is greater than a threshold of 0.004. In other cases, the reflectance measured at 870 nm is subtracted from the measurements in the other bands:

$$\rho_m^{//}(\lambda) = \frac{\rho_0^{//}(\lambda) - \rho_c^{//}(\lambda)}{t_a(\lambda)} - \frac{\rho_0^{//}(870) - \rho_c^{//}(870)}{t_a(870)}. \qquad (16)$$

This formulation assumes the contribution from clouds and whitecaps are spectrally flat across the 443–870 nm spectral range. The assumption is flawed (Frouin et al. 1996), but the use of the rejection threshold minimizes the error introduced by this assumption.

The marine reflectances, $\rho_m(\lambda)$, are then determined from the polarized marine reflectances using a coefficient, $\alpha_{\rm pol}(\lambda)$, which characterizes the polarization rate of the marine signal [see Fougnie et al. (1999a) for more details on the assumptions and justifications involved]. This coefficient was determined at Scripps Institution of Oceanography (SIO) at 450 nm from a Monte Carlo numerical model using a polarized phase function (Zaneveld et al. 1974 and Aas 1981):

$$\rho_m(\lambda) = \frac{\rho_m^{//}(\lambda)}{\alpha_{\rm pol}(\lambda)}, \qquad (17)$$

where the viewing angle is omitted for clarity.

The above-water $L_W(\lambda)$ is defined as follows:

$$\hat{L}_W(\lambda) = \frac{\rho_m(\lambda)}{\pi}E_d(0^+, \lambda), \qquad (18)$$

where π is introduced in the computation of the reflectances during the calibration process. The spectral normalized water-leaving radiance derived from the above-water radiance measurements is:

$$\hat{L}_{WN}(\lambda) = \frac{\rho_m(\lambda)\, E_0(\lambda)}{\pi}\left[\frac{d_0^2}{d^2}\right]. \qquad (19)$$

4.3 SeaPRISM Protocols

The SeaPRISM methodology was the same as the S95 protocol with the following exceptions:

1. Data were collected at three nadir and zenith angles ($\vartheta = 30, 40,$ and $45°$, and $\vartheta' = 150, 140,$ and $135°$, respectively);

2. Data were collected at two azimuth angles (ϕ^+ and ϕ^-); and

3. Three samples for each wavelength were collected at each pointing location (all three samples for a particular wavelength and pointing angle were collected before the next wavelength was sampled).

Table 3. A summary of some of the environmental characteristics of the AAOT site during the SeaPRISM field commissioning including: the chlorophyll a concentration (C_a); the diffuse attenuation coefficient, (K_d); the absorption coefficients due to particulates and yellow substance (a_p and a_y, respectively); and the particulate and yellow substance beam attenuation coefficients (c_p and c_y, respectively). The sea state entries correspond to the World Meteorological Organization (WMO) Code M scale (WMO–N.8). The a, c, and K_d values are all for $\lambda = 490$. The water type classifications are defined according to Loisel and Morel (1998).

Environmental Parameter	SDY 214	SDY†215	SDY 216
Solar Zenith Angle [°]	30.5–55.9	27.6–46.7	27.8–41.4
Wind Speed [$\mathrm{m\,s^{-1}}$]	2.0–3.3	1.5–2.0	2.4–3.3
Sea Roughness (State)	Calm (1)	Calm (1)	Flat (0)
Cloud Cover (Eighths)	Clear (0/8)	Clear (2/8)	Clear (1/8)
Illumination Stability	Stable	Stable	Stable
C_a [$\mathrm{mg\,m^{-3}}$]	1.083	0.929	0.700
K_d [$\mathrm{m^{-1}}$]	0.185	0.180	0.184
$a_p + a_y$ [$\mathrm{m^{-1}}$]	0.095	0.124	0.118
$c_p + c_y$ [$\mathrm{m^{-1}}$]	1.095	1.182	1.064
Water Stratification	Almost None	Almost None	Almost None
Water Type†	Case-1	Case-2	Case-2

† The classification for the sequential day of the year (SDY) 214 is on the Case-1 side of the threshold between Case-1 and Case-2 waters.

The diversity of pointing angles were included so a recommendation for an operational system, based on a quantitative analysis, could be made at the end of an extended field assessment (beyond the short field commissioning).

The three samples permit different formulations for calculating (5) based on the minimum and average of the $L_T(\lambda)$ and $L_i(\lambda)$ data. Because foam and clouds produce brighter than usual radiances for $L_T(\lambda)$ and $L_i(\lambda)$, a simple filter for removing these unwanted effects is to use the minimum values for these data. The three viewing angles, also permit three different types of results, so to keep the preliminary results simple, all of the SeaPRISM data presented hereafter used the minimum value technique and a viewing angle of 40°.

5. PRELIMINARY RESULTS

A summary of the environmental characteristics of the AAOT site during the SeaPRISM field commissioning campaign is given in Table 3. The data were collected primarily in near-ideal conditions: low wind speeds with minimal sea states, and clear skies during stable illumination. Although Case-2 conditions predominated, one day was in Case-1 waters, and the diffuse attenuation coefficient values computed from $E_d(z, \lambda)$ data (K_d) for all days were not excessively large and remained fairly constant.

An important difference in data collection was the (half-angle) FOVs of the above-water instruments: 3.0, 0.6, and 1.5° for the SUnSAS, SeaPRISM, and SIMBAD radiometers, respectively. All of the above-water instruments were mounted or used from the topmost level of the AAOT. Given that each system had a different FOV, and either different or variable nadir angles were used (sometimes purposefully in special SUnSAS experiments or as part of

the programmed SeaPRISM measurement sequence), the area of sea surface being measured was as large as $4.6\,\mathrm{m^2}$, and the distance of the measurement area from the tower base varied from approximately 8.8–11.4 m. A summary of some important instrument sampling characteristics is presented in Table 4.

Table 4. A summary of some of the sampling characteristics for the above- and in-water systems. The FOV values are half angles for the radiance sensors. The time entries represent the amount of time needed to complete one cast.

Sampling System	FOV [°]	Acquisition	
		Rate [Hz]	Time [s]
WiSPER	10.0	6.0	180
miniNESS	10.0	6.0	18
SunSAS†	3.0	6.0	180
SeaPRISM	0.6	1.0	180
SIMBAD	1.5	10.0	10

† An incorrect aperture plate was installed in the sky-viewing radiometer which resulted in a 13°FOV for this sensor.

A summary of the data collected with the above- and in-water instruments is presented in Table 5. The data are arranged chronologically, so the temporal overlap between the sampling systems can be more readily discerned. The relative percent difference between an above- and in-water estimate of water-leaving radiance was computed as:

$$\delta^X(\lambda, t_i) = 100 \frac{\hat{L}_W^X(\lambda, t_i) - \tilde{L}_W(\lambda, t_i)}{\tilde{L}_W(\lambda, t_i)}, \quad (20)$$

where t_i is the time of the measurement, and X is the code for the above-water data collection method (SP for

Table 5. A summary of the SUnSAS, SeaPRISM, SIMBAD, WiSPER, and miniNESS deployment logs. Each entry is composed of a cast number (or name) followed by a temporal range denoting the start and stop times of each cast (the miniNESS entry gives just the start time, because these casts lasted less than 1 min). The reference entry for WiSPER is for the data collected to establish the ratio of the global to indirect solar irradiance. All times are given as a function of the SDY in Greenwich Mean Time (GMT).

SDY	SUnSAS	SeaPRISM	SIMBAD	WiSPER Profiler and Reference	miniNESS	
214			1 1216–1223		P60S1A	1217
					P60S1B	1218
					P60S1C	1219
					P60S1D	1220
					P60S1E	1222
					P60S1F	1225
					P60S1G	1228
					P60S1H	1229
					P60S1I	1230
215				W60S2A 0713–0721	P60S2A	0716
					P60S2B	0717
					P60S2C	0718
					P60S2D	0720
				W60S2B 0721–0728	P60S2E	0722
					P60S2F	0724
					P60S2G	0724
					P60S2H	0725
					P60S2I	0726
	1 0813–0816	1 0810–0813	2 0810–0814	W60S3A 0809–0815	P60S3A	0811
					P60S3B	0812
					P60S3C	0814
					P60S3D	0815
	2 0818–0821	2 0818–0821	3 0818–0822	W60S3B 0816–0823	P60S3E	0817
					P60S3F	0818
					P60S3G	0819
					P60S3H	0822
	3 0828–0831	3 0829–0832	4 0828–0833	W60S3C 0830–0837 W60R2A 0830	P60S3I	0831
	4 0832–0835				P60S3J	0833
					P60S3K	0834
	5 0837–0840	4 0835–0838	5 0836–0841	W60S3D 0837–0845	P60S3L	0836
					P60S3M	0839
	6 0841–0844	5 0841–0844			P60S3N	0842
					P60S3O	0843
	7 0852–0855	6 0852–0855	6 0850–0855	W60S3E 0850–0857	P60S3P	0853
					P60S3Q	0855
	8 0856–0859		7 0857–0900	W60S3F 0857–0904	P60S3R	0856
					P60S3S	0858
	9 0901–0904	7 0859–0902			P60S3T	0859
					P60S3U	0901
					P60S3V	0902
					P60S3W	0903
	10 0905–0908	8 0905–0908	8 0905–0909			
	11 0914–0917	9 0915–0918				
	12 0918–0921					
	13 0922–0925	10 0922–0925	9 0921–0949	W60S3G 0922–0929 W60R3A 0925	P60S3X	0923
					P60S3Y	0926

Table 5. (cont.) A summary of the SUnSAS, SeaPRISM, SIMBAD, WiSPER, and miniNESS deployment logs.

SDY	SUnSAS		SeaPRISM		SIMBAD		WiSPER Profiler	and	Reference		miniNESS	
215	14	0927–0930	11	0929–0932								
	15	0931–0934									P60S3Z	0927
	16	0935–0938	12	0936–0939			W60S3H	0937–0944				
	17	0940–0943										
	18	0945–0948	13	0943–0946					W60R3B	0948		
			14	0949–0952								
	19	1005–1008	15	1005–1008	10	1004–1011	W60S4A	1005–1012	W60R3C	1009	P60S4A	1007
	20	1009–1012									P60S4B	1009
											P60S4C	1010
	21	1013–1016	16	1012–1015	11	1013–1017	W60S4B	1012–1019			P60S4D	1013
											P60S4E	1014
											P60S4F	1016
	22	1018–1021	17	1021–1024	12	1019–1022						
	23	1028–1031	18	1028–1031	13	1027–1034	W60S4C	1028–1035			P60S4G	1029
											P60S4H	1031
	24	1033–1036	19	1035–1038			W60S4D	1035–1042			P60S4I	1034
											P60S4J	1036
											P60S4K	1038
											P60S4L	1039
	25	1045–1048	20	1045–1048	14	1045–1052	W60S4E	1047–1054	W60R3D	1052	P60S4M	1049
	26	1050–1053	21	1052–1055							P60S4N	1052
											P60S4O	1053
	27	1055–1058			15	1055–1058	W60S4F	1054–1101			P60S4P	1057
											P60S4Q	1058
	28	1100–1103	22	1100–1103	16	1100–1104					P60S4R	1100
	29	1109–1112	23	1110–1113	17	1108–1112	W60S4G	1108–1115			P60S4S	1110
											P60S4T	1112
											P60S4U	1113
	30	1114–1117			18	1114–1117	W60S4H	1116–1123			P60S4V	1118
	31	1119–1122	24	1117–1120	19	1119–1126			W60R4A	1122	P60S4W	1119
											P60S4X	1121
	32	1124–1127	25	1124–1127								
									W60R4B	1144		
									W60R4C	1207		
216									W60R4D	1229		
	33	0844–0847	26	0844–0847			W60S5A	0843–0850			P60S5A	0845
	34	0848–0851			20	0848–0856	W60S5B	0850–0856			P60S5B	0851
											P60S5C	0852
	35	0853–0856	27	0852–0855							P60S5D	0853
											P60S5E	0854
											P60S5F	0855
	36	0857–0900	28	0859–0902	21	0857–0901						
	37	0906–0909	29	0907–0910	22	0906–0914	W60S5C	0907–0913			P60S5G	0909
	38	0910–0913									P60S5H	0910
											P60S5I	0912
	39	0915–0918	30	0913–0916			W60S5D	0913–0920			P60S5J	0915
											P60S5K	0916
											P60S5L	0917

Table 5. (cont.) A summary of the SUnSAS, SeaPRISM, SIMBAD, WiSPER, and miniNESS deployment logs.

SDY	SUnSAS		SeaPRISM		SIMBAD		WiSPER Profiler		and	Reference	miniNESS	
216	40	0919–0922	31	0919–0922	23	0918–0922					P60S5M	0919
			32	0926–0929								
	41	0936–0939	33	0939–0942								
	42	0943–0946										
	43	0946–0949	34	0945–0948								
	44	0951–0954	35	0951–0954								
	45	0955–0958	36	0958–1001	24	0955–0959	W60S5E	0954–1001			P60S5N	0956
											P60S5O	0957
											P60S5P	0959
	46	1005–1008	37	1006–1009	25	1001–1007	W60S5F	1001–1008	W60R5A	1001	P60S5Q	1003
											P60S5R	1004
											P60S5S	1005
											P60S5T	1007
	47	1009–1012			26	1008–1012						
	48	1014–1017	38	1013–1016	27	1013–1016						
	49	1018–1020	39	1019–1022								
	50	1023–1026	40	1026–1029					W60R5B	1023		
	51	1041–1044	41	1042–1045	28	1043–1052	W60S6A	1041–1048			P60S6A	1042
											P60S6B	1044
											P60S6C	1045
	52	1046–1049	42	1048–1051			W60S6B	1048–1056			P60S6D	1046
	53	1050–1053									P60S6E	1050
											P60S6F	1051
											P60S6G	1052
	54	1054–1057	43	1055–1058	29	1054–1058						
	55	1103–1106	44	1105–1108	30	1103–1106	W60S6C	1104–1110			P60S6H	1105
											P60S6I	1107
	56	1108–1111	45	1111–1114	31	1108–1111	W60S6D	1111–1118			P60S6J	1108
											P60S6K	1110
											P60S6L	1113
											P60S6M	1114
											P60S6N	1115
											P60S6O	1117
					32	1119–1123						
	57	1124–1127			33	1124–1127	W60S6E	1124–1131	W60R5C	1127	P60S6P	1127
											P60S6Q	1128
	58	1129–1132	46	1127–1130	34	1129–1132					P60S6R	1129
	59	1133–1136	47	1134–1137	35	1134–1138					P60S6S	1133
											P60S6T	1134
											P60S6U	1136
											P60S6V	1137
	60	1138–1141			36	1138–1142					P60S6W	1139
											P60S6X	1141
			48	1143–1146								
	61	1147–1150			37	1147–1151						
	62	1151–1154	49	1150–1153	38	1151–1154						
									W60R6A	1200		
									W60R6B	1220		
									W60R6C	1247		

SeaPRISM and SB for SIMBAD). For the purposes of preliminary analyses, the normalization is made with respect to the WiSPER in-water data, because the objective is to compare the two above-water methods against an independent data set.

To preserve the dispersion of the data during averaging, average percent differences across all coincident measurements were computed using absolute percent differences:

$$\bar{\delta}^X(\lambda) \;=\; \frac{100}{N} \sum_{i=1}^{N} \frac{\left| \hat{L}_W^X(\lambda, t_i) \;-\; \tilde{L}_W(\lambda, t_i) \right|}{\tilde{L}_W(\lambda, t_i)}, \qquad (21)$$

where N is the total number of measurements. The spectral average of the $\bar{\delta}^X(\lambda)$ values was computed as

$$\bar{\psi}^X \;=\; \frac{1}{M} \sum_{j=1}^{M} \bar{\delta}^X(\lambda_j), \qquad (22)$$

where M is the number of channels.

A comparison of water-leaving radiances derived from WiSPER ($\tilde{L}_W$), SeaPRISM ($\hat{L}_W^{SP}$), and SIMBAD ($\hat{L}_W^{SB}$) data are presented in Fig. 13. Three channels (one blue, one green, and one red) common to all three instruments are shown. The SeaPRISM data shows the best agreement with respect to the WiSPER data. The blue-green SIMBAD data are clearly shifted away from the 1:1 line, but the slope of the shift is correct, so the difference is more indicative of a bias.

One source for a bias is in the calibration of the instruments. In a previous intercomparison at the AAOT (Hooker et al. 2000), the instruments involved were intercalibrated using a second generation SeaWiFS Quality Monitor (Hooker et al. 1999). This capability was not available for this field campaign. The SIMBAD and SUn-SAS instruments were calibrated separately and not intercompared in a laboratory setting; the SeaPRISM and WiSPER sensors, however, were calibrated together and, thus, intercompared in the laboratory. Another source of bias is the slightly different wavelengths for each instrument (Fig. 13 inset panel and Table 1).

Histograms of δ values for the Fig. 13 SeaPRISM and SIMBAD data set are given in Figs. 14a and 14b, respectively; spectral averages are given in the inset panels. The SeaPRISM data show the best distribution with respect to the central bin with a well defined and shaped peak centered on the 3–5% bin. The SIMBAD histogram is less defined and centered across the 15–17% and 17–19% bins. The $\bar{\psi}^{SP}$ and $\bar{\psi}^{SB}$ spectral averages for the differences are 8.6 and 13.9%, respectively.

Fig. 13. A comparison of water-leaving radiances between WiSPER, and the SeaPRISM and SIMBAD instruments.
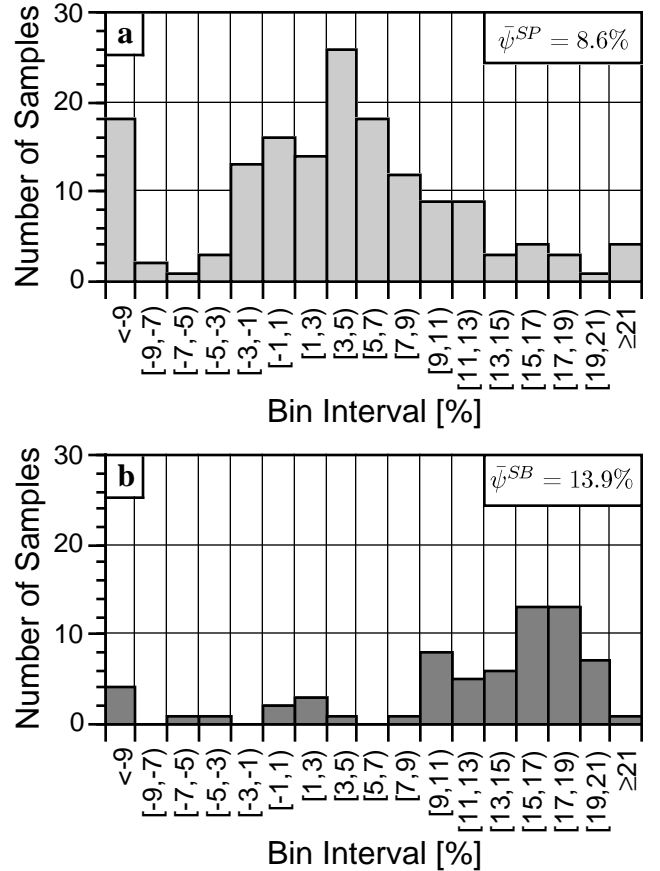
Fig. 14. Histograms of the relative percent differences (δ) between water-leaving radiances derived from WiSPER and **a)** SeaPRISM data, and **b)** SIMBAD data.

Much of the variance (and outliers) in the SeaPRISM differences comes from the red channel, whereas the reverse

is true for the SIMBAD differences. A spectral analysis shows $\bar{\delta}^{SP}(440) = 4.5\%$, $\bar{\delta}^{SP}(500) = 5.9\%$, and $\bar{\delta}^{SP}(670) = 15.6\%$; the corresponding values for the SIMBAD data are 17.7, 15.1, and 8.9%. So the SeaPRISM blue-green channels intercompare with WiSPER at approximately the 5% level, but the SIMBAD blue-green channels intracompare at about the 16% level.

The spectral analysis of the data is one of several possible approaches to the evaluation process. Another technique is to restrict the analysis to $\hat{L}_W(\lambda)$ band ratios, i.e., the 440 and 500 nm ratio for SeaPRISM, and the 443 and 490 ratio for SIMBAD. There are three reasons for considering such an option:

a) Many ocean color algorithms use band ratios as the primary input variable (O'Reilly et al. 1998);

b) Differences in needed (but not applied) corrections (e.g., tower shading) are somewhat mitigated by the normalization process; and

c) Spectral deviations might be persistently biased, that is, parts of the spectrum might be shifted in the same direction and magnitude, so a ratio or normalized analysis might be more satisfactory than a spectral analysis.

The latter is particularly relevant to the above-water methods, because glint contamination elevates broad sections of the spectrum.

The relative percent difference between the band ratios (BR) of an above- and in-water estimate of water-leaving radiance was computed as:

$$\delta_{BR}^X(t_i) = 100 \frac{\dfrac{\hat{L}_W(\lambda_1, t_i)}{\hat{L}_W(\lambda_2, t_i)} - \dfrac{\tilde{L}_W(\lambda_1, t_i)}{\tilde{L}_W(\lambda_2, t_i)}}{\dfrac{\tilde{L}_W(\lambda_1, t_i)}{\tilde{L}_W(\lambda_2, t_i)}}, \quad (23)$$

where $\lambda_1 = 490$ nm and $\lambda_2 = 555$ nm. Averages were formed using the absolute values of $\delta_{BR}^X(t_i)$:

$$\bar{\delta}_{BR}^X = \frac{1}{N} \sum_{i=1}^N |\delta_{BR}^X(t_i)|, \quad (24)$$

where, again, the summation is over the total number of measurements (and spectral averages were not computed, because they are not meaningful).

Figure 15 presents the histograms for the percent differences between the SeaPRISM and SIMBAD band ratio data with respect to the WiSPER band ratio data, δ_{BR}^{SP} and δ_{BR}^{SB}, respectively); absolute difference averages across all the data are given in the inset panels. Although the SeaPRISM results are improved by about a factor of two, in terms of the averages, the SIMBAD results are improved by more than a factor of four. Although both histograms

are much improved with no appreciable outliers, the SIMBAD histogram shows a significantly better shape.
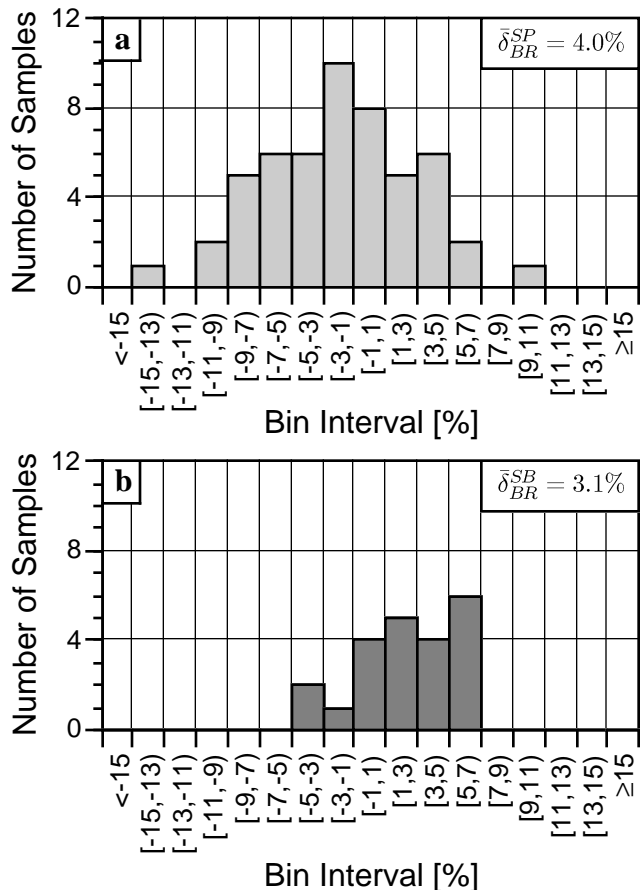
Fig. 15. Histograms of the relative percent difference between the ratio in water-leaving radiances derived from WiSPER and **a)** SeaPRISM data, δ_{BR}^{SP}; and **b)** SIMBAD data, δ_{BR}^{SB}.

6. DISCUSSION

The primary objective of the SeaPRISM field commissioning was to demonstrate the sea-viewing measurement scenario was possible, and to intercompare the water-leaving radiances from SeaPRISM with alternative above- and in-water systems (SIMBAD or SUnSAS and WiSPER, respectively). To provide a quick look at the data collected during the field commissioning, only a portion of the data collected in the experiment was analyzed.

The preliminary results from this effort indicate the following:

1. The agreement between SeaPRISM and WiSPER water-leaving radiances were close to the 5% level in the blue and green parts of the spectrum, but closer to 15% in the red;

2. The SIMBAD spectral comparisons with WiSPER water-leaving radiances were significantly worse (a little more than 15%) than SeaPRISM, although,

the band ratio comparisons were better (approximately 3% for SIMBAD and 4% for SeaPRISM); and

3. Although many of the environmental parameters during the field commissioning were close to ideal (low wind speeds, clear skies, etc.), Case-2 conditions predominated, so agreement at the 5% level and below represents very good agreement.

The last point is important, because the initial data set was composed of only three days of sampling, and these might not be representative of the average capabilities of the SeaPRISM instrument (particularly over an annual cycle which is the standard recalibration interval for the AERONET sun photometers). It is also important to remember the results presented here were for a single viewing angle (40°) and only one processing scheme (the minimum value technique was used).

The excellent preliminary results suggest an extended assessment is appropriate, and some requirements for a fully operational system are worth considering:

a) A maximum number of channels, at the appropriate center wavelengths, for ocean color observations are needed;

b) Programmable viewing angles to satisfy the testing or operational use of different measurement protocols;

c) The collection of a maximum number of sea-viewing values (per measurement sequence and per channel), to ensure statistical robustness for rejecting measurements contaminated by wave, cloud, and sun-glint effects and to maximize the signal-to-noise ratio (particularly in the blue part of the spectrum);

d) Characterization of instrument offsets (dark values) during each measurement sequence; and

e) Automatic transmission of the acquired data over a satellite link (all of the field commissioning data were stored in SeaPRISM and then transferred to a PC through a serial interface).

Although there are limitations associated with some of these recommendations with respect to an automated network, like AERONET, most of the problems have simple and practical solutions.

Acknowledgments

Appendices

A. The SeaPRISM Field Team

Appendix A

SeaPRISM Field Team

The SeaPRISM team members are presented alphabetically.

Sean Bailey
Futuretech Corporation
NASA/GSFC/Code 970.2
Bldg. 28, Room W145
Greenbelt, Maryland 20771
Voice: 301–286–3931
Fax: 301–286–0268
Net: `sbailey@seabass.gsfc.nasa.gov`

Jean-François Berthon
JRC/SAI/ME T.P. 272
Ispra, I–21020 (VA)
ITALY
Voice: 39–0–332–789–934
Fax: 39–0–332–789–034
Net: `jean-francois.berthon@jrc.it`

Pierluigi Cova *and*
Sandro Vianello
CNR/ISDGM
San Polo 1364
I–30125 Venice
ITALY
Voice: 39–0–41–521–6840
Fax: 39–0–41–260–2340
Net: `claudia@neuro.isdgm.ve.cnr.it`

Stanford Hooker
NASA/GSFC/Code 970.2
Bldg. 28, Room W126
Greenbelt, Maryland 20771
Voice: 301–286–9503
Fax: 301–286–0268
Net: `stan@ardbeg.gsfc.nasa.gov`

Dirk van der Linde
JRC/SAI/ME T.P. 272
I–21020 Ispra (VA)
ITALY
Voice: 39–0–332–785–362
Fax: 39–0–332–789–034
Net: `dirk.vanderlinde@jrc.it`

Christophe Pietras
SAIC General Sciences Corporation
NASA/GSFC/Code 970.2
Bldg. 28, Room W119
Greenbelt, Maryland 20771
Voice: 301–286–9892
Fax: 301–286–0268
Net: `pietras@simbios.gsfc.nasa.gov`

Giuseppe Zibordi
JRC/SAI/ME T.P. 272
I–21020 Ispra (VA)
ITALY
Voice: 39–0–332–785–902
Fax: 39–0–332–789–034
Net: giuseppe.zibordi@jrc.it

Glossary

AAOT	*Acqua Alta* Oceanographic Tower
A/D	Analog-to-Digital
AERONET	Aerosol Robotic Network
AMT	Atlantic Meridional Transect
AMT-8	The Eighth AMT Cruise
AOP	Apparent Optical Property
AOT	Aerosol Optical Thickness
ASCII	American Standard Code for Information Interchange
CDOM	Colored Dissolved Organic Matter
CNR	*Consiglio Nazionale delle Ricerche* (National Research Council)
CoASTS	Coastal Atmosphere and Sea Time Series
CTD	Conductivity, Temperature, and Depth
DATA	Not an acronym, but a designator for the Satlantic, Inc., series of power and telemetry units.
DIR	Not an acronym, but a designator for the Satlantic, Inc., series of directional units.
FOV	Field of View
GMT	Greenwich Mean Time
GPS	Global Positioning System
GSFC	Goddard Space Flight Center
HPLC	High Performance Liquid Chromatography
JCR	RRS *James Clark Ross*
JRC	Joint Research Centre
LoCNESS	Low-Cost NASA Environmental Sampling System
miniNESS	miniature NASA Environmental Sampling System
MOBY	Marine Optical Buoy
NASA	National Aeronautics and Space Administration
NRSR	Normalized Remote Sensing Reflectance
OCI	Ocean Color Irradiance
OCR	Ocean Color Radiance
PC	Personal Computer
PM	Particulate Matter
POLDER	Polarization Detecting Environmental Radiometer
RRS	Royal Research Ship
RSMAS	Rosenstiel School for Marine and Atmospheric Science
S/N	Serial Number
SeaBOARR	SeaWiFS Bio-Optical Algorithm Round-Robin
SeaBOARR-98	The First SeaBOARR (held in 1998)
SeaBOARR-99	The Second SeaBOARR (held in 1999)
SeaPRISM	SeaWiFS Photometer Revision for Incident Surface Measurement
SeaWiFS	Sea-viewing Wide Field-of-view Sensor
SDY	Sequential Day of the Year
SIMBAD	Satellite Validation for Marine Biology and Aerosol Determination
SIO	Scripps Institution of Oceanography
SUnSAS	SeaWiFS Underway Surface Acquisition System
THOR	Three-Headed Optical Recorder
TSM	Total Suspended Matter
WiSPER	Wire-Stabilized Profiling Environmental Radiometer
WMO	World Meteorological Organization

Symbols

$a(\lambda)$ The absorption coefficient of seawater.

a_p The absorption coefficient due to particulates.

a_y The absorption coefficient due to yellow substance.

BR A code for identifying a band ratio calculation.

c_p The beam attenuation coefficient due to particulates.

c_y The beam attenuation coefficient due to yellow substance.

C_a The concentration of chlorophyll a.

$C_F(\lambda)$ The (spectral) calibration factor in reflectance per counts.

d^2 The Earth–sun distance of the day.

d_0^2 The Earth–sun distance averaged over the year.

$D^H(\lambda)$ The voltage in counts for the high-level gain.

$D_D^H(\lambda)$ The dark voltage in counts for the high-level gain.

$D^L(\lambda)$ The voltage in counts for the low-level gain.

$D_D^L(\lambda)$ The dark voltage in counts for the low-level gain.

$D_0(\lambda)$ The extraterrestrial solar spectral irradiance in digital counts.

$E(\lambda)$ The direct solar spectral irradiance.

$E_0(\lambda)$ The extraterrestrial solar spectral irradiance.

$E_0'(\lambda)$ The solar irradiances corrected for the solar zenith angle (θ) and the Earth–sun distance.

$E_d(\lambda)$ The downward spectral irradiance.

$E_d(0^+, \lambda)$ The downward spectral irradiance right above the sea surface.

$E_i(\lambda)$ The indirect (diffuse) spectral irradiance.

$E_u(\lambda)$ The upwelled spectral irradiance.

f_{cc} The fractional cloud coverage.

i A numeric index.

j A numeric index.

$K_d(\lambda)$ The diffuse attenuation coefficient calculated from $E_d(z, \lambda)$ data.

$K_u(\lambda)$ The diffuse attenuation coefficient calculated from $L_u(z, \lambda)$ data.

$L_i(\lambda)$ The sky (indirect) spectral radiance.

$L_T(\lambda)$ The total spectral radiance (for $z = 0^+$, right above the sea surface).

$L_u(\lambda)$ The upwelled spectral radiance.

$L_W(\lambda)$ The water-leaving spectral radiance.

$\tilde{L}_W(\lambda)$ The in-water $L_W(\lambda)$ value.

$\tilde{L}_W(\lambda)$ The water-leaving spectral radiance derived from in-water data.

$\hat{L}_W(\lambda)$ The water-leaving spectral radiance derived from above-water radiance measurements.

$\hat{L}_W^X(\lambda)$ The water-leaving spectral radiance derived from above-water method X.

$L_{WN}(\lambda)$ The spectral normalized water-leaving radiance.

$\hat{L}_{WN}(\lambda)$ The spectral normalized water-leaving radiance derived from above-water radiance measurements.

$m(\theta)$ The relative air mass.

M The total number of channels.

$n_w(\lambda)$ The refractive index of seawater.

N The total number of measurements.

SB A code for identifying SIMBAD data.

SP A code for identifying SeaPRISM data.

$t_a(\lambda)$ The atmospheric transmittance (diffuse and direct).

t_i The time of a measurement.

T_C The cloud coverage correction factor.

x The abscissa.

X The above-water method (either SP or SB).

y The ordinate.

z The vertical (depth and altitude) coordinate.

z_0 Center depth.

α The Ångström exponent.

$\alpha_{\mathrm{pol}}(\lambda)$ A coefficient for characterizing the polarization rate of the marine signal.

β The Ångström coefficient.

δz $z - z_0$.

$\delta^X(\lambda)$ The relative percent difference between above-water method X and an in-water (WiSPER) method.

δ_{BR}^X The relative percent difference between band ratios for above-water method X and an in-water (WiSPER) method.

$\bar{\delta}^X(\lambda)$ The average spectral percent difference across all coincident measurements computed using absolute differences for above-water method X.

$\bar{\delta}_{BR}^X$ The average (absolute) percent difference between the band ratio for above-water method X and an in-water (WiSPER) method.

Δz The integration half interval ($\Delta z \approx 4$–$10\,\mathrm{m}$).

θ The solar zenith angle.

ϑ The radiometer pointing (nadir) angle with respect to the vertical axis.

ϑ' $\pi - \vartheta$.

λ Wavelength (the spectral coordinate).

λ_i An individual channel (wavelength).

λ_1 The first wavelength in a band ratio (490 nm).

λ_2 The second wavelength in a band ratio (555 nm).

μ The estimated mean.

ρ' The effective surface reflectance of seawater (0.028).

$\rho(\lambda, \vartheta)$ The Fresnel reflectance of seawater.

$\rho_0(\lambda)$ The observed marine reflectance.

$\rho_m(\lambda)$ The marine reflectance.

$\rho_0^{//}(\lambda)$ The polarized component of the skylight reflectance.

$\rho_c^{//}(\lambda)$ The polarized component of the observed reflectance.

$\rho_m^{//}(\lambda)$ The polarized marine reflectance.

σ The standard deviation.

$\tau(\lambda)$ The spectral total optical thickness.

$\tau_A(\lambda)$ The spectral aerosol optical thickness.

$\tau_C(\lambda)$ The spectral cloud optical thickness.

$\tau_O(\lambda)$ The spectral ozone optical thickness.

$\tau_R(\lambda)$ The spectral Rayleigh optical thickness.

ϕ The solar azimuth angle.

ϕ' $\phi \pm \frac{\pi}{2}$ (90° away from the sun in either direction, i.e., ϕ^+ or ϕ^-).

ϕ^- $\phi - \frac{\pi}{2}$.

ϕ^+ $\phi + \frac{\pi}{2}$.

φ The perturbations (or tilts) in alignment away from z.

$\bar{\psi}^X$ The spectral average of the $\bar{\delta}(\lambda)$ values for above-water method X.

References

Aas, E., 1981: The refractive index of phytoplancton. *Institute for Geophysikk Report Series, No. 46,* Oslo University, 61 pp.

Aiken, J., N. Rees, S. Hooker, P. Holligan, A. Bale, D. Robins, G. Moore, R. Harris, and D. Pilgrim, 2000: The Atlantic Meridional Transect: Overview and synthesis of data. *Prog. Oceanogr.,* **45,** 257–312.

Ångström, A., 1929: On the atmospheric transmission of sun radiation and on dust in the air. *Geogr. Ann.,* **12,** 130–159.

Austin, R.W., 1974: "The remote sensing of spectral radiance from below the ocean surface." In: *Optical Aspects of Oceanography,* N.G. Jerlov and E.S. Nielsen, Eds., Academic Press, London, 317–344.

——, 1980: Gulf of Mexico, Ocean Color Surface Truth Measurements. *Bound.-Layer Meteorol.,* **18,** 269–85.

Deschamps, P.Y., M. Herman, and D. Tanré, 1983: Modeling of the atmospheric effects and its application to the remote sensing of ocean color. *Appl. Opt.,* **22,** 3,751–3,758.

Doyle, J.P., and G. Zibordi, 1998: Correction of oceanographic tower-shading effects on in-water optical measurements. *Proc. Ocean Optics XIV,* [Available on CD-ROM], Office of Naval Research, Washington, DC.

Fougnie, B., R. Frouin, P. Lecompte, P-Y. Deschamps, 1999a: Reduction of skylight reflection effects in the above-water measurements of diffuse marine reflectance. *Appl. Opt.,* **38,** 3,844–3,856.

——, P-Y. Deschamps, R. Frouin, 1999b: Vicarious calibration of the POLDER ocean color spectral bands using *in situ* measurements. *IEEE Trans. Geosci. Remote Sens.,* **37,** 1,567–1,574.

Frouin, R., M. Schwindling, and P.Y. Deschamps, 1996: Spectral reflectance of sea foam in the visible and near infrared: *In situ* measurements and remote sensing implications. *J. Geophys. Res.,* **101,** 14,361–14,371.

Gordon, H.R., and K. Ding, 1992: Self shading of in-water optical instruments. *Limnol. Oceanogr.,* **37,** 491–500.

Holben, B.N., T.F. Eck, I. Slutsker, D. Tanré, J.P. Buis, A. Setzer, E. Vermote, J.A. Reagan, Y.J. Kaufman, T. Nakajima, F. Lavenu, I. Jankowiak, and A. Smirnov, 1998: AERONET—A federated instrument network and data archive for aerosol characterization. *Remote Sens. Environ.,* **66,** 1–16.

Hooker, S.B., G. Zibordi, G. Lazin, and S. McLean, 1999: The SeaBOARR–98 Field Campaign. *NASA Tech. Memo. 1999–206892, Vol. 3,* S.B. Hooker and E.R. Firestone, Eds., NASA Goddard Space Flight Center, Greenbelt, Maryland, 40 pp.

——, and C.R. McClain, 2000: The calibration and validation of SeaWiFS data. *Prog. Oceanogr.,* **45,** 427–465.

——, and G. Lazin, 2000: The SeaBOARR-99 Field Campaign. *NASA Tech. Memo. 2000–206892, Vol. 8,* S.B. Hooker and E.R. Firestone, Eds., NASA Goddard Space Flight Center, 46 pp.

——, and S. Maritorena, 2000: An evaluation of oceanographic radiometers and deployment methodologies. *J. Atmos. Ocean. Tech.,* **17,** 811–830.

——, G. Lazin, G. Zibordi, and S. McLean, 2000: An evaluation of above- and in-water methods for determining water-leaving radiances. *J. Atmos. Ocean. Tech.,* (submitted).

Loisel, H., and A. Morel, 1998: Light scattering and chlorophyll concentration in case 1 waters: A reexamination. *Limnol. Oceanogr.,* **43,** 847–858.

Kasten, F., and A.T. Young, 1989: Revised optical air mass tables: An approximation formula. *Appl. Opt.,* **28,** 4,735–4,738.

Mobley, C.D., 1999: Estimation of the remote-sensing reflectance from above-surface measurements. *Appl. Opt.,* **38,** 7,442–7,455.

Mueller, J.L., and R.W. Austin, 1995: Ocean Optics Protocols for SeaWiFS Validation, Revision 1. *NASA Tech. Memo. 104566, Vol. 25,* S.B. Hooker, E.R. Firestone, and J.G. Acker, Eds., NASA Goddard Space Flight Center, Greenbelt, Maryland, 66 pp.

O'Reilly, J.R., S. Maritorena, B.G. Mitchell, D.A. Siegel, K.L. Carder, S.A. Garver, M. Kahru, and C. McClain, 1998: Ocean color chlorophyll algorithms for SeaWiFS. *J. Geophys. Res.,* **103,** 24,937–24,953.

Robins, D.B., A.J. Bale, G.F. Moore, N.W. Rees, S.B. Hooker, C.P. Gallienne, A.G. Westbrook, E. Marañón, W.H. Spooner, and S.R. Laney, 1996: AMT-1 Cruise Report and Preliminary Results. *NASA Tech. Memo. 104566, Vol. 35,* S.B. Hooker and E.R. Firestone, Eds., NASA Goddard Space Flight Center, Greenbelt, Maryland, 87 pp.

Smith, R.C., and K.S. Baker, 1984: The analysis of ocean optical data. *Ocean Optics VII,* M. Blizard, Ed., SPIE, **478,** 119–126.

——, and ——, 1986: Analysis of ocean optical data II. *Ocean Optics VIII,* P.N. Slater, Ed., SPIE, **637,** 95–107.

Tanré, D., M. Herman, P.Y. Deschamps, and A. de Leffe, 1979: Atmospheric modeling for space measurements of ground reflectances, including bidirectional properties. *Appl. Opt.,* **18,** 213,587–213,597.

Zaneveld, J.R., D.M. Roach, and H. Pak, 1974: The determination of the index of refraction distribution of oceanic particulates. *J. Geophys. Res.,* **79,** 4,091–4,095.

Zibordi, G., and M. Ferrari, 1995: Instrument self-shading in underwater optical measurements: Experimental data. *Appl. Opt.,* **34,** 2,750–2,754.

——, J.P. Doyle, and S.B. Hooker, 1999: Offshore tower shading effects on in-water optical measurements. *J. Atmos. Ocean. Tech.,* **16,** 1,767–1,779.

——, J-F. Berthon, J.P. Doyle, S. Grossi, D.W. van der Linde, C. Targa, L. Alberotanza, and P. Cova, 2000: Coastal Atmosphere and Sea Time Series (CoASTS): A long-term field project for satellite color data validation in the North Adriatic Sea. *J. Geophys. Res.,* (submitted).

The SeaWiFS Postlaunch Technical Report Series

Vol. 1

Johnson, B.C., J.B. Fowler, and C.L. Cromer, 1998: The Sea-WiFS Transfer Radiometer (SXR). *NASA Tech. Memo. 1998–206892, Vol. 1,* S.B. Hooker and E.R. Firestone, Eds., NASA Goddard Space Flight Center, Greenbelt, Maryland, 58 pp.

Vol. 2

Aiken, J., D.G. Cummings, S.W. Gibb, N.W. Rees, R. Woodd-Walker, E.M.S. Woodward, J. Woolfenden, S.B. Hooker, J-F. Berthon, C.D. Dempsey, D.J. Suggett, P. Wood, C. Donlon, N. González-Benítez, I. Huskin, M. Quevedo, R. Barciela-Fernandez, C. de Vargas, and C. McKee, 1998: AMT-5 Cruise Report. *NASA Tech. Memo. 1998–206892, Vol. 2,* S.B. Hooker and E.R. Firestone, Eds., NASA Goddard Space Flight Center, Greenbelt, Maryland, 113 pp.

Vol. 3

Hooker, S.B., G. Zibordi, G. Lazin, and S. McLean, 1999: The SeaBOARR-98 Field Campaign. *NASA Tech. Memo. 1999–206892, Vol. 3,* S.B. Hooker and E.R. Firestone, Eds., NASA Goddard Space Flight Center, Greenbelt, Maryland, 40 pp.

Vol. 4

Johnson, B.C., E.A. Early, R.E. Eplee, Jr., R.A. Barnes, and R.T. Caffrey, 1999: The 1997 Prelaunch Radiometric Calibration of SeaWiFS. *NASA Tech. Memo. 1999–206892, Vol. 4,* S.B. Hooker and E.R. Firestone, Eds., NASA Goddard Space Flight Center, Greenbelt, Maryland, 51 pp.

Vol. 5

Barnes, R.A., R.E. Eplee, Jr., S.F. Biggar, K.J. Thome, E.F. Zalewski, P.N. Slater, and A.W. Holmes 1999: The Sea-WiFS Solar Radiation-Based Calibration and the Transfer-to-Orbit Experiment. *NASA Tech. Memo. 1999–206892, Vol. 5,* S.B. Hooker and E.R. Firestone, Eds., NASA Goddard Space Flight Center, 28 pp.

Vol. 6

Firestone, E.R., and S.B. Hooker, 2000: SeaWiFS Postlaunch Technical Report Series Cumulative Index: Volumes 1–5. *NASA Tech. Memo. 2000–206892, Vol. 6,* S.B. Hooker and E.R. Firestone, Eds., NASA Goddard Space Flight Center, Greenbelt, Maryland, 14 pp.

Vol. 7

Johnson, B.C., H.W. Yoon, S.S. Bruce, P-S. Shaw, A. Thompson, S.B. Hooker, R.E. Eplee, Jr., R.A. Barnes, S. Maritorena, and J.L. Mueller, 1999: The Fifth SeaWiFS Intercalibration Round-Robin Experiment (SIRREX-5), July 1996. *NASA Tech. Memo. 1999–206892, Vol. 7,* S.B. Hooker and E.R. Firestone, Eds., NASA Goddard Space Flight Center, 75 pp.

Vol. 8

Hooker, S.B., and G. Lazin, 2000: The SeaBOARR-99 Field Campaign. *NASA Tech. Memo. 2000–206892, Vol. 8,* S.B. Hooker and E.R. Firestone, Eds., NASA Goddard Space Flight Center, 46 pp.

Vol. 9

McClain, C.R., E.J. Ainsworth, R.A. Barnes, R.E. Eplee, Jr., F.S. Patt, W.D. Robinson, M. Wang, and S.W. Bailey, 2000: SeaWiFS Postlaunch Calibration and Validation Analyses, Part 1. *NASA Tech. Memo. 2000–206892, Vol. 9,* S.B. Hooker and E.R. Firestone, Eds., NASA Goddard Space Flight Center, 82 pp.

Vol. 10

McClain, C.R., R.A. Barnes, R.E. Eplee, Jr., B.A. Franz, N.C. Hsu, F.S. Patt, C.M. Pietras, W.D. Robinson, B.D. Schieber, G.M. Schmidt, M. Wang, S.W. Bailey, and P.J. Werdell, 2000: SeaWiFS Postlaunch Calibration and Validation Analyses, Part 2. *NASA Tech. Memo. 2000–206892, Vol. 10,* S.B. Hooker and E.R. Firestone, Eds., NASA Goddard Space Flight Center, 57 pp.

Vol. 11

O'Reilly, J.E., and 24 Coauthors, 2000: SeaWiFS Postlaunch Calibration and Validation Analyses, Part 3. *NASA Tech. Memo. 2000–206892, Vol. 11,* S.B. Hooker and E.R. Firestone, Eds., NASA Goddard Space Flight Center, 49 pp.

Vol. 12

Firestone, E.R., and S.B. Hooker, 2000: SeaWiFS Postlaunch Technical Report Series Cumulative Index: Volumes 1–11. *NASA Tech. Memo. 2000–206892, Vol. 12,* S.B. Hooker and E.R. Firestone, Eds., NASA Goddard Space Flight Center, Greenbelt, Maryland, (in preparation).

Vol. 13

Hooker, S.B., G. Zibordi, J-F. Berthon, S.W. Bailey, and C.M. Pietras, 2000: The SeaWiFS Photometer Revision for Incident Surface Measurement (SeaPRISM) Field Commissioning. *NASA Tech. Memo. 2000–206892, Vol. 13,* S.B. Hooker and E.R. Firestone, Eds., NASA Goddard Space Flight Center, Greenbelt, Maryland, 24 pp.